On mineral dust aerosol hygroscopicity

Lanxiadi Chen,[1,6] Chao Peng,[1] Athanasios Nenes,[2,5] Wenjun Gu,[1,6] Hanjing Fu,[3] Xing Jian,[3] Huanhuan Zhang,[1,6] Guohua Zhang,[1] Jianxi Zhu,[4] Xinming Wang,[1,6,7] Mingjin Tang[1,6,7,*]

[1] State Key Laboratory of Organic Geochemistry and Guangdong Key Laboratory of Environmental Protection and Resources Utilization, Guangzhou Institute of Geochemistry, Chinese Academy of Sciences, Guangzhou, China

[2] Laboratory of Atmospheric Processes and their Impacts, School of Architecture, Civil & Environmental Engineering, École Polytechnique Fédérale de Lausanne (EPFL), Lausanne, Switzerland

[3] State Key Laboratory of Marine Environmental Science, College of Ocean and Earth Sciences, Xiamen University, Xiamen, China

[4] CAS Key Laboratory of Mineralogy and Metallogeny and Guangdong Provincial Key Laboratory of Mineral Physics and Material Research and Development, Guangzhou Institute of Geochemistry, Chinese Academy of Sciences, Guangzhou, China

[5] Institute of Chemical Engineering Sciences, Foundation for Research & Technology-Hellas, Patras, Greece

[6] University of Chinese Academy of Sciences, Beijing, China

[7] Center for Excellence in Regional Atmospheric Environment, Institute of Urban Environment, Chinese Academy of Sciences, Xiamen, China

* Correspondence: Mingjin Tang (mingjintang@gig.ac.cn)

Abstract

Despite its importance, hygroscopicity of mineral dust aerosol remains highly uncertain. In this work, we investigated water adsorption and hygroscopicity of different mineral dust samples at 25 ^{o}C, via measurement of sample mass at different relative humidity (RH, up to 90%) using a vapor sorption analyzer. Mineral dust samples examined (21 in total) included seven authentic mineral dust samples from different regions in the world and fourteen major minerals contained in mineral dust aerosol. At 90% RH, the mass ratios of adsorbed water to the dry mineral ranged from 0.0011 to 0.3080, largely depending on the BET surface areas of mineral dust samples. The fractional surface coverages of adsorbed water were determined to vary between 1.26 and 8.63 at 90% RH, and it was found that the Frenkel-Halsey-Hill (FHH) adsorption isotherm could well describe surface coverages of adsorbed water as a function of RH, with A_{FHH} and B_{FHH} parameters in the range of 0.15-4.39 and 1.10-1.91, respectively. The comprehensive and robust data obtained would largely improve our knowledge of hygroscopicity of mineral dust aerosol.

1 Introduction

Mineral dust aerosol mainly comes from arid and semi-arid areas (Ginoux et al., 2012), such as Saharan desert, Taklimakan desert, and etc. Its annual flux and atmospheric loadings are estimated to be ~2000 Tg yr^{-1} and ~19.2 Tg (Textor et al., 2006; Huneeus et al., 2011), making mineral dust one of the most important aerosols in the troposphere. Mineral dust aerosol has significant impacts on atmospheric chemistry, climate and biogeochemical cycles (Knippertz and Stuut, 2014). It can alter the radiative forcing of the earth both directly (Balkanski et al., 2007; Huang et al., 2014; Di Biagio et al., 2017) and indirectly (Cziczo et al., 2013; Karydis et al., 2017). Mineral dust can also change the abundance of reactive trace gases as well as aerosol compositions via heterogeneous reactions (Usher et al., 2003; Dupart et al., 2012; He et al., 2014; Tang et al., 2017; Yu and Jang, 2019). Furthermore, the deposition of mineral dust will bring substantial amounts of nutrients (e.g., Fe and P) into some marine and terrestrial ecosystems, thereby largely affecting biogeochemistry in these regions (Jickells et al., 2005; Okin et al., 2011; Schulz et al., 2012; Li et al., 2017; Tagliabue et al., 2017; Meskhidze et al., 2019).

Hygroscopicity largely determines the impacts of mineral dust aerosol on atmospheric chemistry and climate. For examples, many studies found that relative humidity (RH) and thus the amount of water associated with mineral dust have profound effects on the rates, mechanisms and products of heterogeneous reactions (Vlasenko et al., 2009; Rubasinghege and Grassian, 2013; Tang et al., 2014; Tang et al., 2017; Lasne et al., 2018; Wang et al., 2018; Yu and Jang, 2018; Mitroo et al., 2019). In addition, hygroscopicity of mineral dust aerosol plays important roles in its optical properties (and thus the direct radiative effect) and its ability to act as cloud condensation nuclei and ice-nucleating particles (and thus the indirect radiative effect) (Sorjamaa and Laaksonen, 2007; Kumar et al., 2009; Garimella et al., 2014; Kreidenweis and Asa-Awuku, 2014; Laaksonen

et al., 2016; Tang et al., 2016; Tang et al., 2019a). Therefore, a number of previous studies have investigated water adsorption and hygroscopic properties of mineral dust aerosol at <100% RH, as reviewed by Tang et al. (2016). However, different studies displayed considerable discrepancies as large as a few orders of magnitude (Tang et al., 2016), thus precluding a good understanding of the roles mineral dust aerosol plays in atmospheric chemistry and climate.

As pointed out by Tang et al. (2016), such discrepancies are largely due to the non-sphericity and low hygroscopicity of mineral dust particles, making it difficult to quantify the amount of water associated with them at elevated RH. Instruments which measure mobility or optical diameters of aerosol particles often found that the diameters of mineral dust particles did not increase significantly (or even showed considerable decrease due to particle restructuring during humidification) with increasing RH (Gustafsson et al., 2005; Vlasenko et al., 2005; Herich et al., 2009; Koehler et al., 2009; Attwood and Greenslade, 2011). Fourier transform infrared spectroscopy (FTIR) is a sensitive method to detect adsorbed water on mineral dust (Goodman et al., 2001; Ma et al., 2010a; Joshi et al., 2017); however, it is not a trivial task to convert the intensity of its infrared absorption to the amount of adsorbed water (Schuttlefield et al., 2007b; Ma et al., 2010b; Tang et al., 2016). Quartz crystal microbalance (QCM) is another sensitive technique to examine water adsorption and absorption (Schuttlefield et al., 2007b; Navea et al., 2010; Yeşilbaş and Boily, 2016); however, it is in doubt that the underlying assumptions required to convert the change in resonance frequency of the quartz crystal to the change in sample mass are always fulfilled (Tang et al., 2016; Tang et al., 2019a).

In our previous work (Gu et al., 2017), we developed a new method to investigate hygroscopic properties of atmospherically relevant particles using a vapor sorption analyzer, which utilized a very sensitive balance to measure the mass of a sample (typically with a dry mass

of tenths or a few mg) as different RH under isotherm conditions. Comprehensive validation carried out confirmed the robustness of this method (Gu et al., 2017), and this instrument has been employed to study hygroscopic properties of various particles, including nonspherical particles such as saline mineral dust and pollen grains (Chen et al., 2019; Tang et al., 2019b; Tang et al., 2019c). This instrument was used in the present work to quantitively investigate hygroscopic properties of a number of mineral dust particles, including several authentic mineral dust samples from different regions in the world and individual minerals commonly found in mineral dust aerosol. We also attempted to figure out which theoretical models could describe hygroscopic properties of mineral dust particles, and examined the dependence of mineral dust hygroscopicity on several parameters (such as particle diameter, surface area and the mass fraction of soluble materials).

2 Experimental section

2.1 Sample information

In total 21 different types of mineral dust were investigated, including fourteen major minerals commonly found in mineral dust aerosol (Formenti et al., 2011; Nickovic et al., 2012; Journet et al., 2014; Scanza et al., 2015; Engelbrecht et al., 2016) and seven authentic mineral dust samples, and their information can be found in Table 1. The fourteen major minerals examined included four oxides (SiO_2, TiO_2, magnetite and hematite), one oxyhydroxide (goethite), three feldspars (potassium feldspar, albite and microcline), two carbonates ($CaCO_3$ and dolomite) and four clay minerals (montmorillonite, illite, kaolinite and chlorite). As shown in Table 1, SiO_2, montmorillonite and kaolinite were supplied by Sigma Aldrich; TiO_2 (P25) was supplied by Degussa; hematite and magnetite were supplied by Strem; goethite was provided by Santa Cruz; microcline, $CaCO_3$ and dolomite were provided by Alfa Aesar. Potassium feldspar and albite were

obtained from National Research Center of Testing Techniques for Building Materials (NRCTTBM, Beijing, China), and illite (IMt-1) was obtained from the Clay Mineral Society at Purdue University, Indianan, USA (Schuttlefield et al., 2007b; Tang et al., 2014). In addition, chlorite was collected by one co-author from Liaoning Province, China.

Table 1. Measured BET surface areas (BET), average particle diameters (d_p) and sources of mineral dust samples examined in this work.

sample	BET (m^2/g)	d_p (μm)	source
SiO_2	6.54 ±0.01	1.65 ±0.30	Sigma Aldrich
TiO_2	54.60 ±0.01	1.66 ±0.31	Degussa
hematite	9.23 ±0.17	0.80 ±0.13	Strem
goethite	13.41 ±0.01	1.00 ±0.21	Santa Cruz
magnetite	6.34 ±0.04	1.70 ±0.33	Strem
potassium feldspar	3.96 ±0.01	8.25 ±1.57	NRCTTBM
albite	3.62 ±0.02	5.51 ±1.05	NRCTTBM
microcline	2.17 ±0.01	14.33 ±1.87	Alfa Aesar
$CaCO_3$	2.18 ±0.01	3.12 ±0.56	Alfa Aesar
dolomite	11.79 ±0.05	7.41 ±1.42	Alfa Aesar
illite	24.04 ±0.14	20.23 ±2.42	The Clay Minerals Society
kaolinite	9.64 ±0.01	9.99 ±1.45	Sigma Aldrich
montmorillonite	249.91 ±0.42	23.95 ±2.49	Sigma Aldrich
chlorite	9.95 ±0.03	19.19 ±2.27	Liaoning, China
ATD	36.67 ±1.06	1.05 ±0.20	Powder Technology Inc.
China loess	11.71 ±0.02	2.44 ±0.42	Chinese Academy of Geological Science
QH dust	8.79 ±0.02	18.56 ±2.38	Chinese Academy of Geological Science
TLF dust	8.49 ±0.01	8.04 ±1.46	Turpan, Xinjiang, China
Bordj dust	16.40 ±1.20	32.30 ±3.06	Bordj, Senegal
M'Bour dust	14.50 ±1.00	54.41 ±5.99	M'Bour, Algeria
Saharan dust	51.46 ±0.34	23.70 ±2.59	Cape Verde

The seven authentic mineral dust samples were obtained from Africa, Asia and North America. As shown in Figure 1, three authentic mineral dust samples (M'Bour dust, Bordj dust and Saharan dust) were collected from topsoil in Senegal, Algeria and Cape Verde Islands (Tang et al., 2012; Joshi et al., 2017), respectively. QH dust (which is brown desert soil) and China loess, collected from topsoil in Qinghai and Shaanxi, were supplied by Chinese Academy of Geological Science as certificated materials (GBW07448 and GBW07454) (Tang et al., 2019c). TLF dust were airborne dust particles collected on 23 April 2010 at an urban site in Turpan (Xinjiang, China) during a major dust storm. In addition, Arizona Test Dust (ATD, nominal 0-3 μm fraction), an authentic mineral dust sample commercially available from Powder Technology Inc. (Minnesota, USA) and widely used in atmospheric aerosol research (Vlasenko et al., 2005; Sullivan et al., 2010a; Tang et al., 2016), was also investigated in our work.

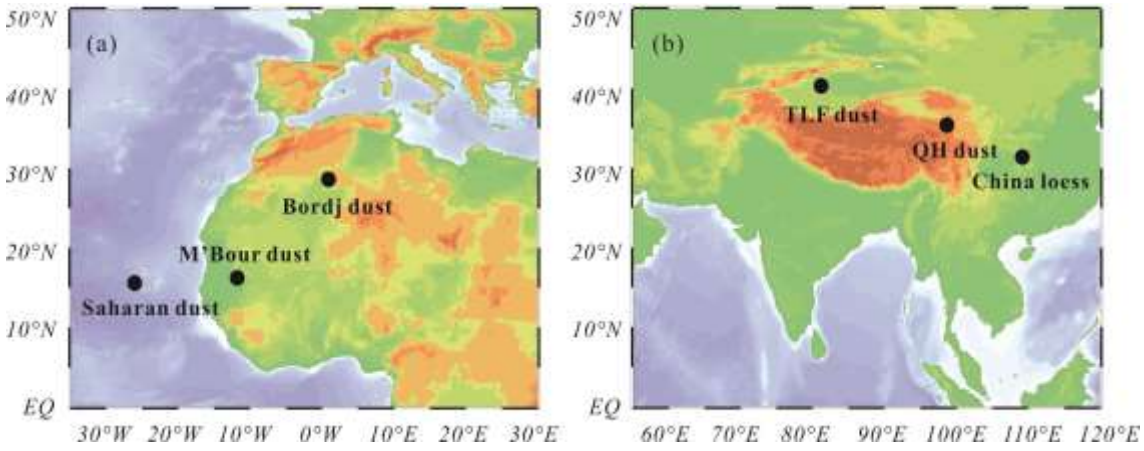

Figure 1. Locations where (a) African and (b) Asian authentic mineral dust samples examined in this work were collected.

When received, three feldspars, dolomite, illite, chlorite and TLF dust contained significant amounts of rock chips or giant particles; as a result, they were pretreated using the procedure described in our previous work (Tang et al., 2019c). In brief, these samples were dried at 120 ^{o}C

for 24 hours using an oven; after that, they were ground manually and then using a ball mill so that most particles were <74 μm in diameter; finally, these samples were dried again at 120 ^{o}C for 24 hours and then cooled down. All the samples were stored in plastic bottles which were tightly sealed to prevent contamination by lab air.

2.2 Sample characterization

Dynamic light scattering (JL-1177, Jingxin Powder Technologies Inc., Chengdu, Sichuan, China) was employed to measure size distributions of mineral dust samples examined in our work. In addition, Brunauer-Emmett-Teller (BET) surface areas of these samples were determined using an accelerated surface area and porosimetry analyzer (ASAP 2020 PLUS, Micromeritics, Georgia, USA), and N_2 was used as the adsorbate. Details on particle size and BET surface area measurements can be found elsewhere (Li et al., 2020).

To measure their inorganic soluble compositions, each mineral dust sample (~10 mg) was mixed with 10 mL ultrapure deionized water, and the mixture was stirred for 2 hours using an oscillating table. After centrifugalization, the solution was filtered using a 5 mL syringe fitted with a 0.2 μm PTFE membrane syringe and then analyzed using ion chromatography (Metrohm model 761 Compact IC, Metrohm, Herisau, Switzerland). More information on ion chromatography analysis can be found in our previous work (Tang et al., 2019c). We attempted to measure five cations (Na^+, K^+, NH_4^+, Mg^{2+} and Ca^{2+}) and seven anions (NO_3^-, SO_4^{2-}, Cl^-, NO_2-, Br^-, F^- and PO_4^{3-}), and their detection limits were estimated to be around 0.02 mg/L.

2.3 Hygroscopicity measurements

Hygroscopic properties of mineral dust samples were investigated using a vapor sorption analyzer (Q5000SA, TA instruments, Delaware, USA). This instrument, described in our previous work (Gu et al., 2017; Chen et al., 2019; Tang et al., 2019b), measured sample mass as a function

of RH under isotherm conditions. Measurements could be conducted in the RH range of 0-98% and in the temperature range of 5-85 °C. We routinely measured the deliquescence RH of NaCl, $(NH_4)_2SO_4$ and KCl at 25 °C, and the measured values differed from the actual values by <1% RH. The sample mass could be measured with an accuracy of ±0.1 μg, and the uncertainties for temperature and RH were ±0.1 °C and ±1%.

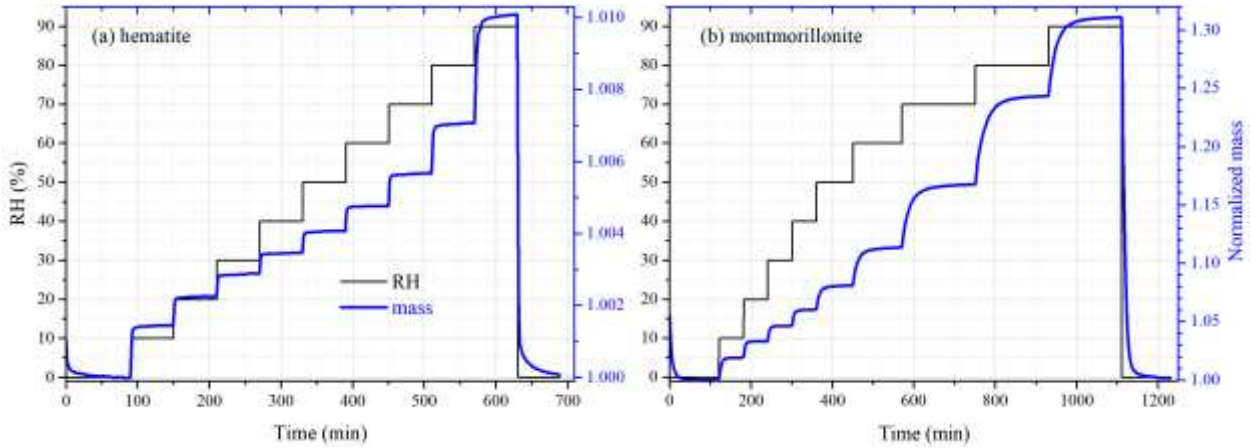

Figure 2. RH (black curve, left *y*-axis) and mass of mineral dust (normalized to that at <1% RH, blue curve, right *y*-axis) as a function of experimental time: (a) hematite; (b) montmorillonite.

In this work, the initial masses of mineral dust samples used typically ranged from 5 to 15 mg. As displayed in Figure 2, the sample under investigation was first dried at <1% RH; after that, RH was increased in a stepwise manner to 90%, and at each step RH was increased by 10%; at last, the sample was dried again at <1% RH. At each step we changed the RH only after the samples mass became stable (in other words, only after an equilibrium was reached between gaseous and particulate water), and the sample mass was considered to be stable when the mass change was <0.05% in 30 min. In some experiments the sample was considered to reach the equilibrium only when the mass change was <0.05% in 60 min, and no significant difference in results was found for the two equilibrium criterions. All the experiments were carried out in triplicate at 25 °C.

3 Results

3.1 Sample characteristics

As shown in Table 1, the BET surface areas were found to vary between 2.17±0.01 m^2/g (microcline) and 249.91±0.42 m^2/g (montmorillonite), spanning over two orders of magnitude. Except for montmorillonite, the BET surface areas were in the range of a few to tens of m^2/g. In addition, the average particle diameters (d_p) were determined to range from 0.80 μm (hematite) to 54.41 μm (M'Bour dust), and their size distributions can be found in Figures S1-S7.

Tables S1-S2 show mass fractions of water soluble inorganic ions for the 21 mineral dust samples considered in this study. Na^+, K^+, Ca^{2+}, Mg^{2+}, F^-, Cl^- and SO_4^{2-} were detected in most of the samples, while NH_4^+ was above its detection limit only for two samples. The total mass fractions of all the soluble inorganic ions were found to be quite low, ranging from 0.16 mg/g for SiO_2 and 12.55 mg/g for Bordj dust.

3.2 Water uptake by different mineral dust

As described in Section 2.3, sample mass of mineral dust was measured at different RH in our work; therefore, the mass ratio of adsorbed water to the dry mineral, m_w/m_0, could then be determined as a function of RH. Furthermore, m_w/m_0 could be converted to fractional surface coverage (abbreviated as surface coverage) of adsorbed water (θ), using Eq. (1) (Tang et al., 2016):

$$\theta = \frac{m_w}{m_0} \cdot \frac{N_A \cdot A_w}{M_w \cdot A_{BET}} \qquad (1),$$

where N_A is Avogadro constant (6.02×10^{23} mol^{-1}), M_w is the molar mass of water (18 g mol^{-1}), A_w is the surface area each adsorbed water molecule would occupy (assumed to be 1×10^{-15} cm^2) (Schuttlefield et al., 2007a; Hatch et al., 2014; Tang et al., 2016), and A_{BET} is the BET surface (in cm^2 g^{-1}) of the mineral dust under consideration. Tables 2-5 summarize m_w/m_0 and θ as a function of RH for all the mineral dust examined in our work. Please note that our previous work (Tang et

al., 2019c) discussed water uptake by China loess and QH dust, and these results are included here to compare with the other nineteen mineral dust samples.

Table 2. Mass ratios of adsorbed water to the dry mineral (m_w/m_0) and surface coverages of adsorbed water (θ) as a function of RH (%) for SiO_2, TiO_2, magnetite, hematite, goethite and potassium feldspar.

RH	SiO_2		TiO_2		hematite	
	m_w/m_0 ($\times10^{-3}$)	θ	m_w/m_0 ($\times10^{-3}$)	θ	m_w/m_0 ($\times10^{-3}$)	θ
10	0.5±0.1	0.25±0.02	3.1±1.1	0.19±0.07	1.4±0.1	0.52±0.02
20	0.8±0.1	0.40±0.05	5.4±1.2	0.33±0.07	2.2±0.1	0.81±0.03
30	1.1±0.1	0.55±0.05	7.2±1.2	0.44±0.07	2.9±0.1	1.03±0.04
40	1.4±0.1	0.70±0.05	8.9±1.2	0.54±0.07	3.4±0.2	1.24±0.06
50	1.7±0.1	0.86±0.06	10.8±1.2	0.66±0.08	4.0±0.2	1.46±0.07
60	2.0±0.1	1.04±0.07	13.5±1.3	0.82±0.08	4.7±0.2	1.72±0.07
70	2.6±0.2	1.32±0.09	16.8±1.3	1.03±0.08	5.7±0.2	2.06±0.07
80	3.5±0.3	1.81±0.14	21.8±1.3	1.34±0.08	7.1±0.2	2.56±0.07
90	5.8±0.7	2.95±0.35	35.5±1.3	2.17±0.08	10.1±0.2	3.68±0.08
RH	goethite		magnetite		potassium feldspar	
	m_w/m_0 ($\times10^{-3}$)	θ	m_w/m_0 ($\times10^{-3}$)	θ	m_w/m_0 ($\times10^{-3}$)	θ
10	1.3±0.1	0.33±0.02	0.5±0.1	0.27±0.01	0.6±0.1	0.54±0.01
20	2.2±0.2	0.55±0.04	0.7±0.1	0.39±0.07	1.0±0.1	0.84±0.01
30	2.9±0.2	0.73±0.06	1.0±0.1	0.52±0.08	1.5±0.3	1.24±0.25
40	3.7±0.5	0.92±0.12	1.2±0.1	0.64±0.07	1.7±0.3	1.46±0.25
50	4.4±0.5	1.10±0.12	1.5±0.1	0.77±0.07	2.0±0.3	1.70±0.24
60	5.2±0.5	1.30±0.12	1.8±0.1	0.93±0.07	2.3±0.2	1.92±0.17
70	6.1±0.4	1.53±0.11	2.2±0.1	1.15±0.07	2.7±0.2	2.25±0.17
80	7.5±0.4	1.88±0.10	2.9±0.1	1.55±0.04	3.5±0.2	2.92±0.19
90	12.4±0.4	3.09±0.11	5.2±0.3	2.72±0.16	5.6±0.3	4.73±0.21

Below we discuss hygroscopicity of mineral dust investigated, and compare our measured m_w/m_0 and θ with those reported in previous work. As our work directly measured mass change of mineral dust due to water uptake, we prefer to compare m_w/m_0 when such values were also reported in previous studies; otherwise, we then choose to compare θ. As aerosol-based measurements are usually not sensitive enough and also need the particle sphericity assumption (Tang et al., 2016), we do not compare our results with those measurements.

3.2.1 SiO_2 and TiO_2

In our work m_w/m_0 was determined to be 0.0011, 0.0020 and 0.0058 for SiO_2 at 30%, 60% and 90% RH, corresponding to θ of 0.55, 1.04 and 2.95, respectively. Figure 3a compares our work with previous studies in which FTIR (Goodman et al., 2001; Ma et al., 2010a; Joshi et al., 2017) and QCM (Schuttlefield et al., 2007a; Yeşilbaş and Boily, 2016) were used to measure water uptake by SiO_2. At a given RH, θ values reported by the four previous studies (Goodman et al., 2001; Schuttlefield et al., 2007a; Ma et al., 2010a; Joshi et al., 2017) were generally larger when compared to our work, and the difference usually did not exceed a factor of three. Furthermore, the differences between our work and the four previous studies became smaller at higher RH. For example, at 80% RH our measured θ was very close to those reported by Ma et al. (2010a) and Joshi et al. (2017), and at 90% RH our measured θ was 20-30% larger than those reported by the two studies (Ma et al., 2010a; Joshi et al., 2017). Yeşilbaş and Boily (2016) employed a QCM to investigate water adsorption on quartz (0.3-14 μm), and θ was determined to be ~2300 at ~70% RH, almost three orders of magnitude larger than these reported in our work and other previous studies (Goodman et al., 2001; Schuttlefield et al., 2007a; Ma et al., 2010a; Joshi et al., 2017); therefore, the results reported by Yeşilbaş and Boily (2016) are not displayed in Figure 3a.

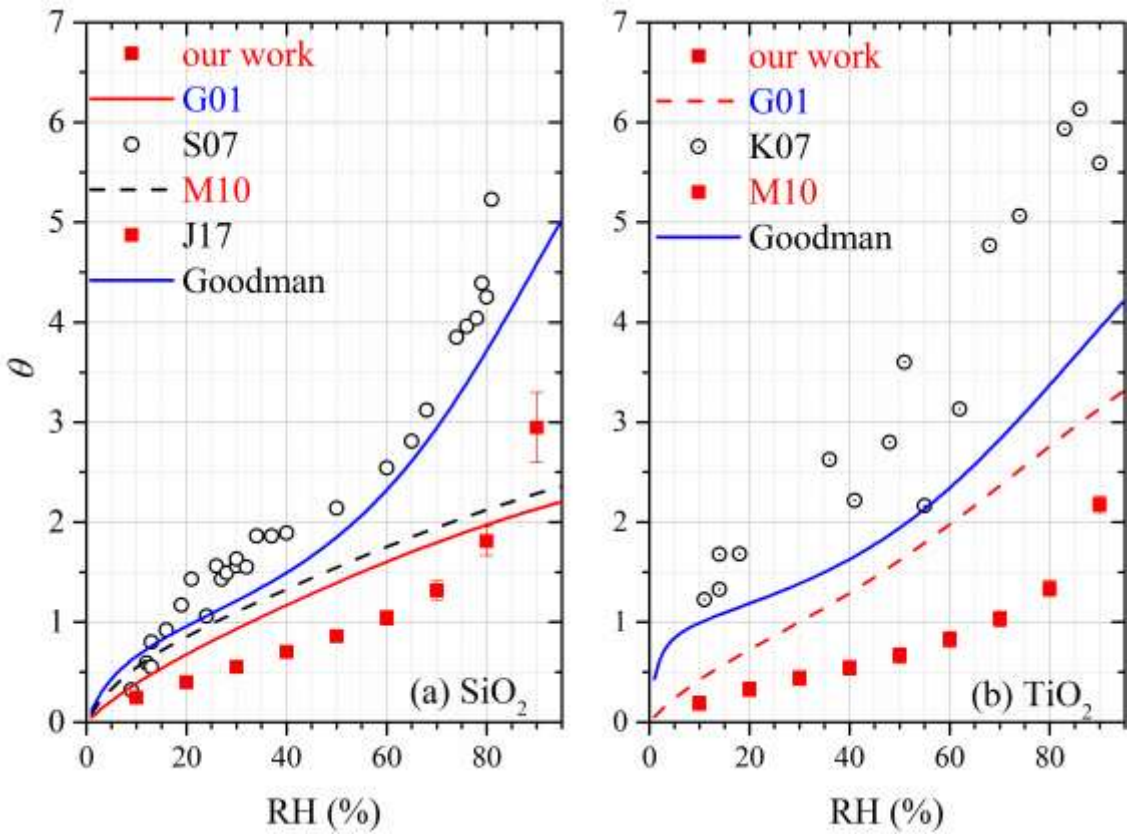

Figure 3. Comparison of surface coverages of adsorbed water (θ) measured in our work with those reported in previous studies for (a) SiO_2 and (b) TiO_2. G01: Goodman et al. (2001); S07: Schuttlefield et al., 2007a; M10: Ma et al., 2010a; J17: Joshi et al., 2017; K07: Ketteler et al., 2007.

For TiO_2, m_w/m_0 was determined to be 0.0072, 0.0135 and 0.0355 at 30%, 60% and 90% RH, corresponding to θ of 0.44, 0.82 and 2.17, respectively. Water adsorption on P25 TiO_2 was studied previously using FTIR (Goodman et al., 2001; Ma et al., 2010a), and another study (Ketteler et al., 2007) employed atmospheric pressure X-ray photoelectron spectroscopy to explore interactions of water vapor with the rutile single crystal surface (110). As shown in Figure 3b, when compared with our work, θ values reported by Ma et al. (2010a) were higher across the entire RH range, and the relative differences between our work and Ma et al. (2010a) were around a factor of two or smaller. The relative differences between our work and the other two studies

(Goodman et al., 2001; Ketteler et al., 2007) were larger, being a factor of ~5 at lower RH and becoming smaller at higher RH.

3.2.2 Hematite, goethite and magnetite

At 30%, 60% and 90% RH, m_w/m_0 was measured to be 0.0029, 0.0047 and 0.0101 for hematite, corresponding to θ of 1.03, 1.72 and 3.68. Water adsorption on hematite was studied previously using FTIR (Goodman et al., 2001; Ma et al., 2010a) and QCM (Yeşilbaş and Boily, 2016). Figure 4a reveals that our results agreed reasonably well with those reported by Goodman et al. (2001) and Ma et al. (2010a), and the relative differences were found to be within a factor of two. In addition, our results agreed fairly well with those reported for 10 nm hematite by Yeşilbaş and Boily (2016), but were significantly smaller than their results for 50 nm hematite. Yeşilbaş and Boily (2016) also studied water adsorption on 4 and 5 μm hematite particles, and θ were reported to be ~300 at ~70% RH, almost two orders of magnitude larger than our results; therefore, their measured θ for 4 and 5 μm hematite are not shown in Figure 4a.

In our work, m_w/m_0 was measured to be 0.0029, 0.0052 and 0.0124 at 30%, 60% and 90% RH for goethite, corresponding to θ of 0.73, 1.30 and 3.09. Yeşilbaş and Boily (2016) employed QCM to study water adsorption on goethite, and their measured θ are plotted in Figure 4b to compare ours. When compared to our work, on average θ values measured by Yeşilbaş and Boily (2016) were a factor of ~2 larger. We also investigated water adsorption on magnetite, and the results can be found in Figure 4b. Compared to goethite, θ values were generally 20-30% smaller for magnetite. As far as we know, water adsorption on magnetite was not quantitatively investigated before.

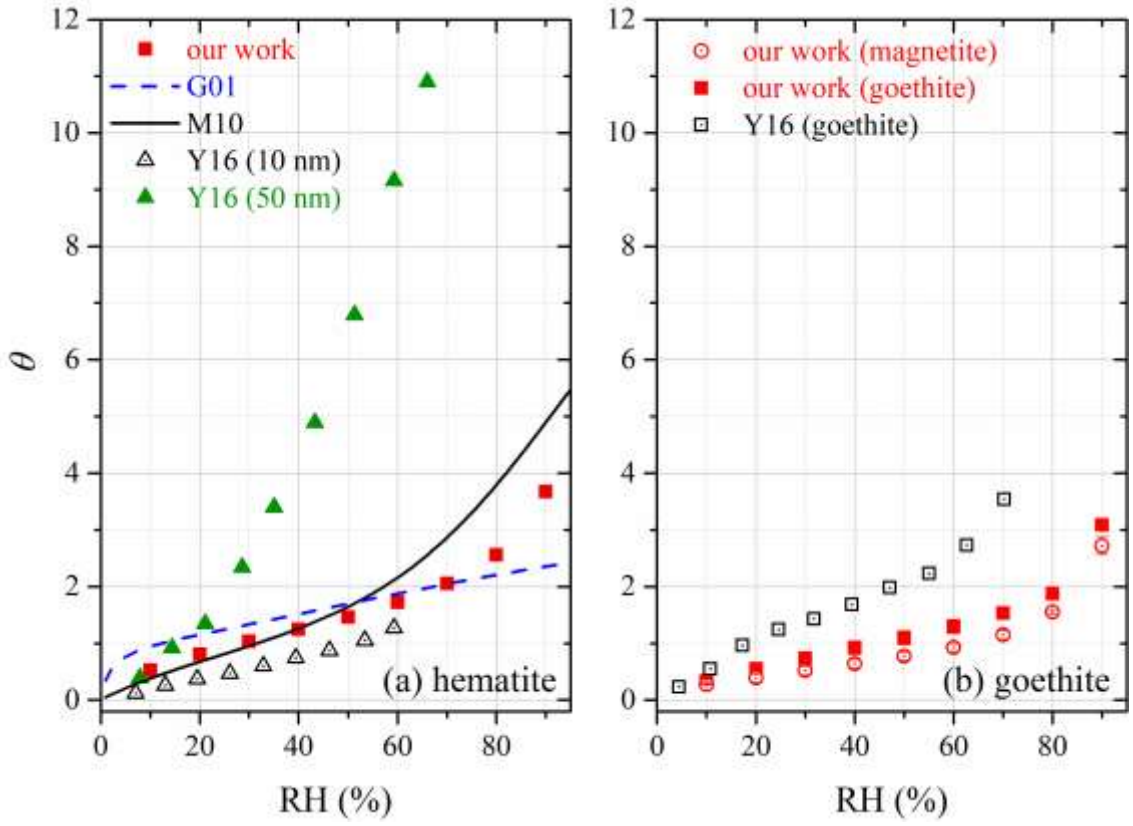

Figure 4. Comparison of surface coverages of adsorbed water (θ) measured in our work with those reported in previous studies for (a) hematite and (b) goethite (θ measured in our work for magnetite are also plotted). G01: Goodman et al. (2001); M10: Ma et al., 2010a; Y16, Yeşilbaş and Boily, 2016.

3.2.3 Feldspars

Tables 2-3 show that the mass ratios of adsorbed water to the dry mineral were determined to be 0.0056, 0.0060 and 0.0048 at 90% RH for potassium feldspar, albite and microcline, respectively; correspondingly, θ were found to be 4.73, 5.53 and 7.37. QCM was used by Yeşilbaş and Boily (2016) to study water uptake onto microcline, and θ was measured to be ~300 at ~70% RH, about two orders of magnitude larger than our measurement. We are not aware of other previous studies which investigated water adsorption on feldspars in a quantitative manner.

Table 3. Mass ratios of adsorbed water to the dry mineral (m_w/m_0) and surface coverages of adsorbed water (θ) as a function of RH (%) for albite, microcline, $CaCO_3$, dolomite, illite and kaolinite.

RH	albite		microcline		$CaCO_3$	
	m_w/m_0 ($\times10^{-3}$)	θ	m_w/m_0 ($\times10^{-3}$)	θ	m_w/m_0 ($\times10^{-3}$)	θ
10	0.7±0.2	0.67±0.20	0.3±0.1	0.51±0.10	0.1±0.1	0.10±0.07
20	1.1±0.2	1.00±0.19	0.5±0.1	0.81±0.14	0.2±0.2	0.27±0.24
30	1.3±0.1	1.19±0.04	0.7±0.1	1.06±0.19	0.2±0.2	0.38±0.28
40	1.6±0.1	1.45±0.04	0.8±0.2	1.28±0.26	0.2±0.1	0.33±0.17
50	1.9±0.1	1.74±0.04	1.0±0.2	1.57±0.29	0.3±0.1	0.41±0.22
60	2.3±0.1	2.10±0.03	1.4±0.2	2.11±0.30	0.4±0.2	0.63±0.31
70	2.8±0.1	2.63±0.05	1.9±0.1	2.96±0.22	0.5±0.2	0.79±0.34
80	3.8±0.1	3.50±0.06	2.8±0.2	4.40±0.33	0.7±0.3	1.02±0.39
90	6.0±0.1	5.53±0.06	4.8±0.6	7.37±0.98	1.1±0.5	1.73±0.79
RH	dolomite		illite		kaolinite	
	m_w/m_0 ($\times10^{-3}$)	θ	m_w/m_0 ($\times10^{-3}$)	θ	m_w/m_0 ($\times10^{-3}$)	θ
10	0.4±0.1	0.13±0.02	5.0±0.1	0.69±0.01	1.4±0.3	0.48±0.10
20	0.7±0.1	0.21±0.02	8.3±0.1	1.15±0.01	2.4±0.4	0.83±0.14
30	0.9±0.1	0.26±0.04	11.0±0.1	1.53±0.01	3.2±0.5	1.12±0.17
40	1.1±0.2	0.31±0.05	13.5±0.2	1.88±0.03	4.0±0.6	1.38±0.20
50	1.3±0.2	0.36±0.06	15.7±0.2	2.18±0.03	4.7±0.7	1.63±0.23
60	1.5±0.2	0.42±0.06	18.1±0.5	2.52±0.07	5.6±0.8	1.95±0.27
70	1.8±0.3	0.51±0.08	21.0±0.7	2.93±0.09	7.0±0.9	2.43±0.32
80	2.5±0.5	0.70±0.15	25.3±0.7	3.52±0.10	9.3±1.0	3.22±0.36
90	4.5±0.5	1.26±0.14	33.3±0.7	4.63±0.10	14.6±1.1	5.08±0.39

3.2.4 Carbonates

283 The mass ratio of adsorbed water to the dry mineral, m_w/m_0, was measured in our work to
284 be 0.0011 at 90% RH for $CaCO_3$, giving a θ value of 1.73. Water adsorption on $CaCO_3$ was
285 investigated previously, using thermogravimetric analysis (Gustafsson et al., 2005), physisorption
286 analysis (Ma et al., 2012a) and QCM (Hatch et al., 2008; Schuttlefield, 2008; Yeşilbaş and Boily,
287 2016). Hatch et al. (2008) and Ma et al. (2008) reported m_w/m_0 as a function of RH. Figure 5a
288 shows that when compared to our work, m_w/m_0 values determined by Hatch et al. (2008) were
289 significantly larger (by a factor of 10 or more), whereas the results reported by Ma et al. (2012)
290 were only smaller by a factor of ~2. We further compare our measured θ with those reported by
291 another two studies (Gustafsson et al., 2005; Schuttlefield, 2008). As shown in Figure 5b, the
292 results reported by Gustafsson et al. (2005) and Schuttlefield (2008) were found to be larger than
293 ours, by a factor of 2-3. In addition, θ was measured to be >100 at ~70% RH for $CaCO_3$ (Yeşilbaş
294 and Boily, 2016), approximately two orders of magnitude larger than our work.
295 As shown in Table 3, our work suggested that around 1.26 monolayers of adsorbed water
296 was formed on dolomite at 90% RH, similar to that for $CaCO_3$. To our knowledge, water
297 adsorption on dolomite has not been quantitatively explored by previous work.

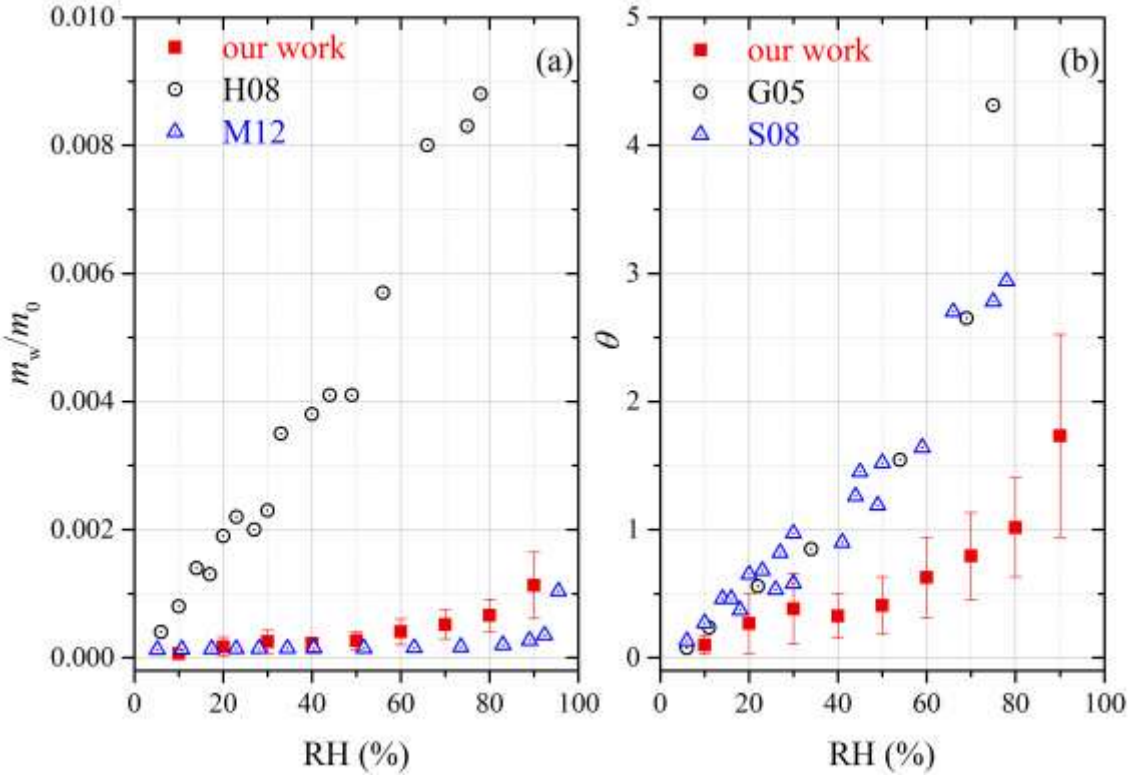

Figure 5. Comparison of water adsorption on $CaCO_3$ examined in different studies: (a) mass ratios of adsorbed water to the dry mineral (m_w/m_0); (b) surface coverages of adsorbed water (θ). G05, Gustafsson et al. (2005); H08, Hatch et al. (2008); S08, Schuttlefield (2008); M12, Ma et al. (2012).

3.2.5 Clay minerals

For illite, m_w/m_0 and θ were determined to be 0.0333 and 4.63 at 90% RH in our study (Table 3). QCM was employed to study water adsorption on illite, and m_w/m_0 was reported to be 0.28 at ~90% RH (Hatch et al., 2011) and ~0.27 at 75% RH (Schuttlefield et al., 2007b), around one order of magnitude larger than our results. A recent study (Yeşilbaş and Boily, 2016) also investigated water uptake onto illite using QCM, and their reported θ are compared with our results in Figure 6a. The relative differences between our and their (Yeşilbaş and Boily, 2016) work were usually smaller than a factor of two, and became even smaller at higher RH.

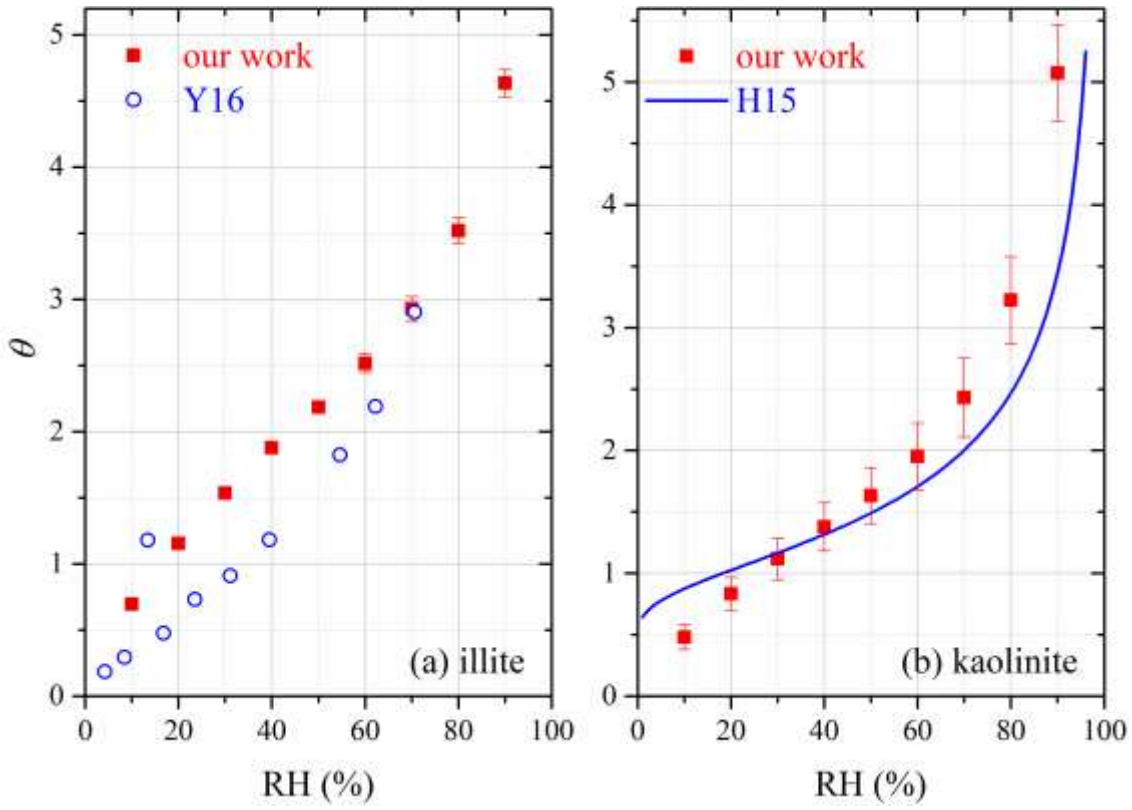

Figure 6. Comparison of surface coverages of adsorbed water (θ) measured by different studies for (a) illite and (b) kaolinite. H15, Hung et al. (2015); Y16, Yeşilbaş and Boily (2016).

For kaolinite, m_w/m_0 and θ were determined in our work to 0.0093 and 3.22 at 80% RH and 0.0146 and 5.08 at 90% RH, respectively. A few previous studies investigated water adsorption on kaolinite using QCM (Schuttlefield et al., 2007b; Hatch et al., 2011; Yeşilbaş and Boily, 2016) and physisorption analysis (Hung et al., 2015). Comparison with our measured θ with those reported by Hung et al. (2015) is displayed in Figure 6b for kaolinite, suggesting that the two studies were in good agreement, and the relative differences were usually within 30%. At ~80% RH, m_w/m_0 were determined to be ~0.03 for kaolinite provided by Alfa and ~0.1 for kaolinite (KGa-1b) obtained from Clay Mineral Society (Schuttlefield et al., 2007b), around three and ten times larger than our work. In the work by Hatch et al. (2011), m_w/m_0 was determined to be ~0.1

at ~80% RH for kaolinite (KGa-1b), about one order of magnitude larger than our result. Yeşilbaş and Boily (2016) examined water adsorption on two different kaolinite samples (kaolinite provided by Fluka and KGa-1), and θ were found to be up to 100 at ~70% RH, being >30 times larger than our work.

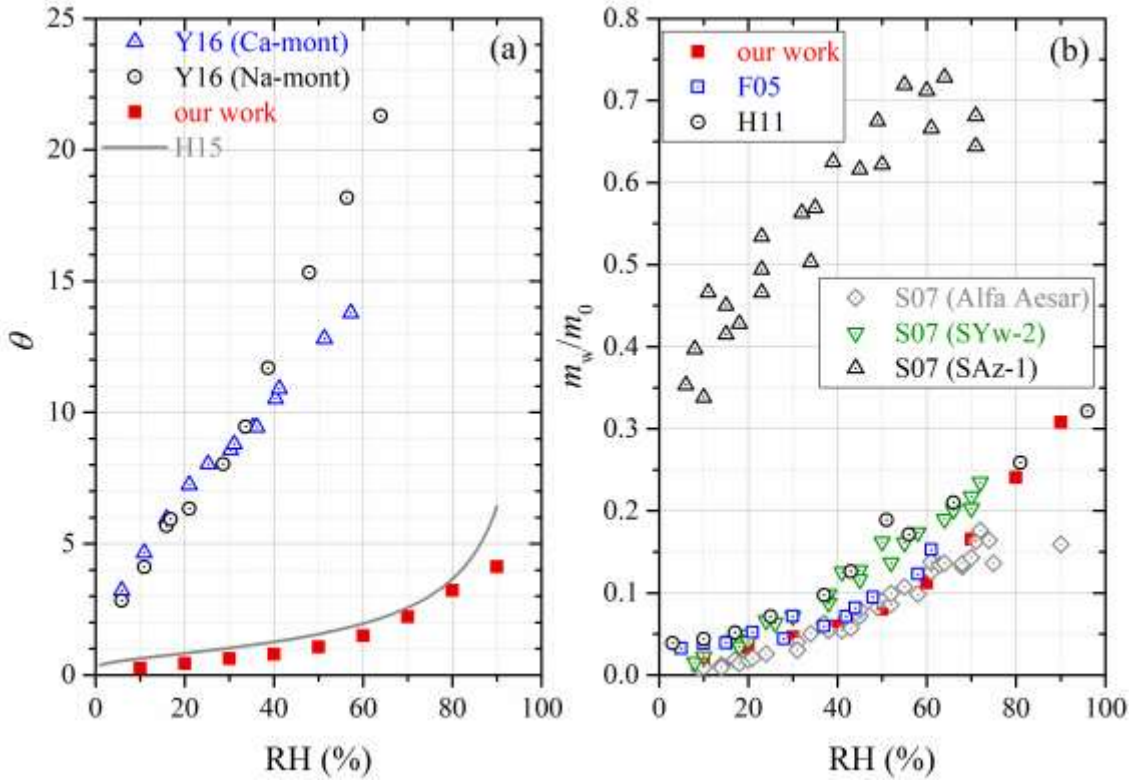

Figure 7. Comparison of water adsorption on montmorillonite examined in different studies: (a) surface coverages of adsorbed water (θ); (b) the mass ratio of adsorbed water to the dry mineral (m_w/m_0). F05, Frinak et al. (2005); S07, Schuttlefield et al. (2007); H11, Hatch et al. (2011); H15, Hung et al. (2015); Y16, Yeşilbaş and Boily (2016).

We also studied water adsorption on montmorillonite, and m_w/m_0 and θ were measured to be 0.308 and 4.12 at 90% RH. Physisorption analysis (Hung et al., 2015) and QCM (Yeşilbaş and Boily, 2016) were utilized to investigate water uptake onto montmorillonite. As shown in Figure

7a, our work agreed well with Hung et al. (2015), and the results obtained by Yeşilbaş and Boily (2016) for Ca- and Na-montmorillonite were much larger (by a factor of >10), when compared with our work. Figure 7b compares our measured m_w/m_0 with those reported in previous studies in which FTIR (Frinak et al., 2005) and QCM (Schuttlefield et al., 2007b; Hatch et al., 2011) were used. In general good agreement between our work and the three previous studies were found, except for SAz-1 montmorillonite (Schuttlefield et al., 2007b) obtained from Clay Mineral Society. One possible explanation for the observed discrepancy is that montmorillonite samples from different sources may have different hygroscopic properties. We note that prior to 2005, a few studies (Hall and Astill, 1989; Cases et al., 1992; Xu et al., 2000; Zent et al., 2001) also investigated water uptake by montmorillonite, and it was found that these studies agreed well with Frinak et al. (2005); therefore, the four studies conducted before 2005 should also be consistent with our work.

In addition, water uptake by chlorite was explored in our work. As shown in Table 4, m_w/m_0 and θ were measured to be 0.012 and 4.03 at 90% RH. To our knowledge, hygroscopic properties of chlorite have not been examined before.

Table 4. Mass ratio of adsorbed water to the dry mineral (m_w/m_0) and surface coverages of adsorbed water (θ) as a function of RH (%) for montmorillonite, chlorite, ATD, M'Bour dust, Bordj dust and Saharan dust.

RH	montmorillonite		chlorite		ATD	
	m_w/m_0 ($\times10^{-3}$)	θ	m_w/m_0 ($\times10^{-3}$)	θ	m_w/m_0 ($\times10^{-3}$)	θ
10	19.2 ±0.2	0.26 ±0.01	1.3 ±0.1	0.42 ±0.02	9.9 ±0.1	0.90 ±0.01
20	33.3 ±0.3	0.45 ±0.01	2.1 ±0.1	0.70 ±0.03	16.1 ±0.2	1.47 ±0.02
30	46.3 ±0.4	0.62 ±0.01	2.8 ±0.1	0.94 ±0.04	20.9 ±0.1	1.91 ±0.01
40	59.7 ±0.8	0.80 ±0.01	3.4 ±0.1	1.14 ±0.04	25.3 ±0.1	2.31 ±0.01
50	80.2 ±0.9	1.07 ±0.01	4.0 ±0.1	1.34 ±0.05	29.6 ±0.1	2.70 ±0.01

60	112.5 ±1.1	1.51 ±0.02	4.7 ±0.1	1.57 ±0.05	34.1 ±0.1	3.11 ±0.01
70	165.4 ±2.3	2.21 ±0.03	5.7 ±0.1	1.93 ±0.05	39.4 ±0.1	3.59 ±0.01
80	240.7 ±2.5	3.22 ±0.03	7.7 ±0.1	2.57 ±0.05	47.0 ±0.3	4.29 ±0.03
90	308.0 ±2.9	4.12 ±0.04	12.0 ±0.2	4.03 ±0.08	64.4 ±0.9	5.87 ±0.08

RH	M'Bour dust		Bordj dust		Saharan dust	
	m_w/m_0 ($\times10^{-3}$)	θ	m_w/m_0 ($\times10^{-3}$)	θ	m_w/m_0 ($\times10^{-3}$)	θ
10	1.4 ±0.1	0.31 ±0.01	1.0 ±0.1	0.21 ±0.01	10.2 ±0.2	0.66 ±0.02
20	2.3 ±0.1	0.54 ±0.01	2.0 ±0.5	0.41 ±0.09	16.6 ±0.4	1.02 ±0.03
30	3.2 ±0.1	0.73 ±0.02	2.6 ±0.5	0.53 ±0.09	21.4 ±0.2	1.39 ±0.01
40	3.9 ±0.3	0.90 ±0.07	3.4 ±0.4	0.69 ±0.08	26.0 ±0.2	1.69 ±0.01
50	4.6 ±0.4	1.06 ±0.10	4.0 ±0.4	0.82 ±0.08	30.4 ±0.3	1.98 ±0.02
60	5.2 ±0.5	1.21 ±0.13	5.0 ±0.4	1.02 ±0.09	36.0 ±0.2	2.34 ±0.02
70	6.9 ±0.6	1.59 ±0.13	7.6 ±0.5	1.55 ±0.10	43.8 ±0.3	2.84 ±0.02
80	9.2 ±0.6	2.13 ±0.14	11.8 ±0.4	2.41 ±0.08	55.7 ±0.7	3.62 ±0.05
90	15.2 ±0.5	3.51 ±0.11	19.2 ±0.3	3.91 ±0.07	79.3 ±1.5	5.15 ±0.10

3.2.6 Authentic mineral dust

ATD: Table 4 suggests that at 90% RH, m_w/m_0 and θ were measured in our work to be 0.0644 and 5.87 for ATD. Two previous studies (Navea et al., 2010; Yeşilbaş and Boily, 2016) employed QCM to investigate water adsorption on ATD. In the first study (Navea et al., 2010), m_w/m_0 was measured to be >0.1 at 70% RH, being 2-3 times larger than our result (~0.04 at 70% RH); in the second study (Yeşilbaş and Boily, 2016), θ was measured to be >200 at ~70% RH, almost two orders of magnitude larger than our work (~3.6 at 70% RH). Gustafsson et al. (2005) used a thermogravimetric analyzer to study water uptake by ATD, and as shown in Figure 8a, their results agreed very well with ours. A recent study (Joshi et al., 2017) investigated water adsorption on ATD using FTIR; compared to our work, the values reported by Joshi et al. (2017) were ~30% lower, suggesting fairly good agreement between the two studies.

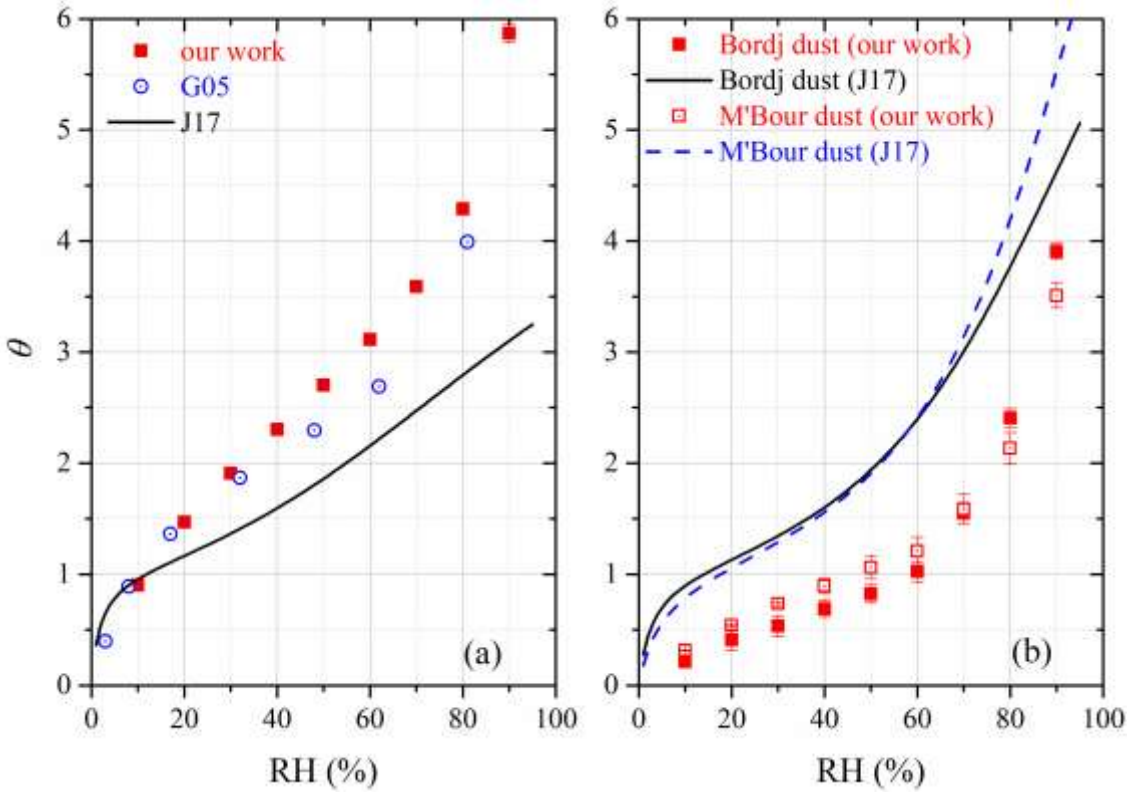

Figure 8. Comparison of surface coverages of adsorbed water (θ) reported in different studies for (a) ATD and (b) Bordj dust and M'Bour dust. G05, Gustafsson et al. (2005); J17, Joshi et al. (2017).

African dust: In our study, m_w/m_0 and θ were measured to be 0.0192 and 3.91 for Bordj dust and 0.0152 and 3.51 for M'Bour dust at 90% RH, respectively. Joshi et al. (2017) employed FTIR to investigate interaction of water vapor with Bordj dust and M'Bour dust. As suggested by Figure 8b, the relative differences between our and their work (Joshi et al., 2017) were usually within a factor of two for the two dust samples, and the discrepancy also became smaller at higher RH, suggesting fair consistence between the two studies.

For Saharan dust, m_w/m_0 and θ were determined in our study to be 0.0793 and 5.15 at 90% RH. Water uptake onto Saharan dust was studied using QCM (Navea et al., 2010), and their results, as shown in Figure 9a, were 2-3 times larger than our work.

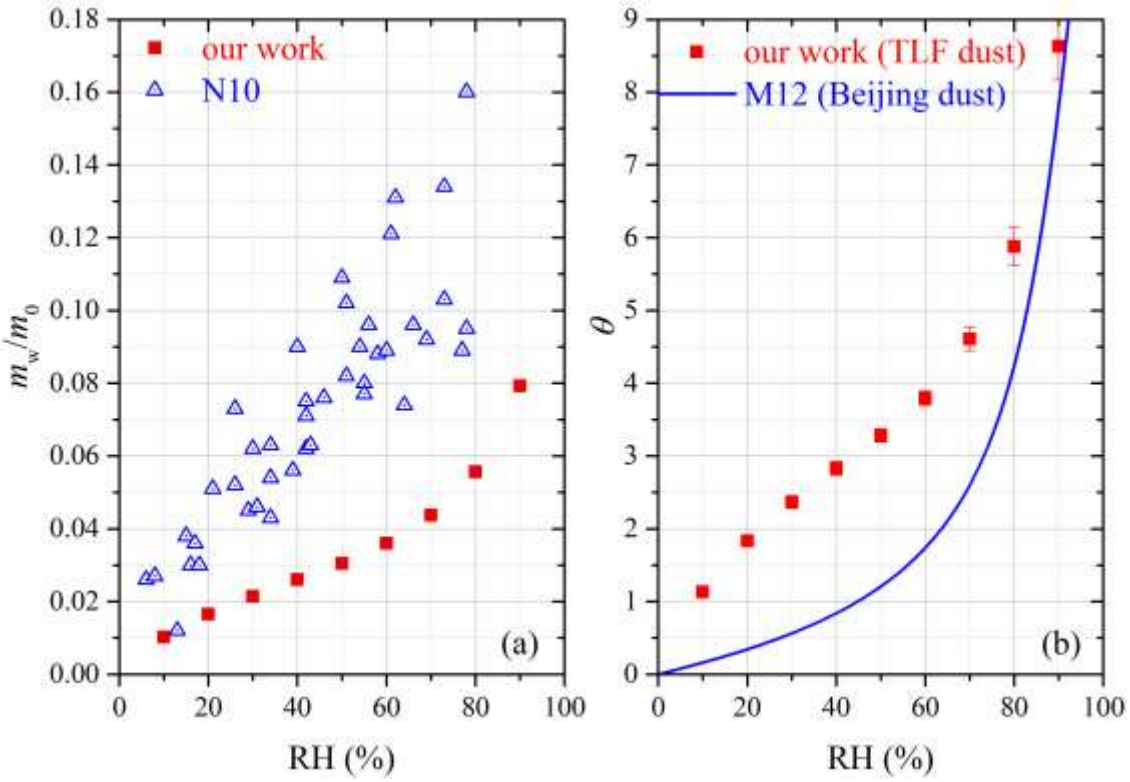

Figure 9. (a) Comparison of mass ratios of adsorbed water to the dry mineral (m_w/m_0) measured by our work and N10 (Navea et al., 2010) for Saharan dust. (b) Comparison of surface coverages of adsorbed water (θ) for TLF dust measured in our work with Beijing dust measured in M12 (Ma et al., 2012b).

Asian dust: Table 5 summarizes our results obtained for three Asian mineral dust samples, including China loess, QH dust and TLF dust. It should be pointed out that m_w/m_0 have been reported in our previous work (Tang et al., 2019c) for China loess and QH dust, and they are included here for comparison. As shown in Table 5, the three Asian authentic dust samples exhibited very similar water uptake properties, and their m_w/m_0 were determined to be 0.021-0.022 at 90% RH. Navea et al. (2010) employed QCM to study interaction of water vapor with China

loess, and m_w/m_0 was reported to be ~0.17 at 70% RH, more than one order of magnitude larger than our result (~0.012 at 70% RH).

As mentioned in Section 2.1, TLF dust examined in our work were airborne dust particles collected during a dust storm in Turpan (Xinjiang, China) which was very close to the dust source. In a previous study (Ma et al., 2012b), dust particles (termed as Beijing dust here) were collected during a dust storm in Beijing (and thus these particles had undergone atmospheric aging to some extent), and their hygroscopic properties were then investigated using a physisorption analyzer. As revealed by Figure 9b, our work agreed fairly well with Ma et al. (2012b) at high RH (70%, 80% and 90%), though the differences became considerably larger at lower RH.

Table 5. Mass ratios of adsorbed water to the dry mineral (m_w/m_0) and surface coverages of adsorbed water (θ) as a function of RH (%) for QH dust, China loess and TLF dust.

RH	QH dust		China loess		TLF dust	
	m_w/m_0 ($\times10^{-3}$)	θ	m_w/m_0 ($\times10^{-3}$)	θ	m_w/m_0 ($\times10^{-3}$)	θ
10	2.2±0.1	0.84±0.01	3.0±0.1	0.87±0.03	2.9±0.1	1.13±0.05
20	3.7±0.1	1.39±0.01	4.9±0.1	1.39±0.04	4.7±0.2	1.83±0.08
30	4.9±0.1	1.86±0.01	6.2±0.1	1.78±0.04	6.0±0.2	2.37±0.09
40	6.0±0.1	2.29±0.01	7.4±0.1	2.12±0.03	7.2±0.2	2.83±0.09
50	7.2±0.1	2.75±0.01	8.7±0.2	2.49±0.04	8.3±0.2	3.28±0.09
60	8.6±0.1	3.29±0.01	10.2±0.2	2.90±0.04	9.6±0.3	3.79±0.11
70	10.4±0.1	3.96±0.01	11.9±0.2	3.41±0.05	11.7±0.4	4.61±0.16
80	13.4±0.1	5.09±0.02	14.6±0.2	4.17±0.05	14.9±0.7	5.88±0.26
90	21.5±0.1	8.20±0.01	21.2±0.3	6.05±0.07	21.9±1.2	8.63±0.46

3.2.7 Discussion

To investigate water adsorption by mineral dust, one previous study (Gustafsson et al., 2005) employed thermogravimetric analysis which measured sample mass as a function of RH

(essentially the same to VSA used in our study), and another two groups (Ma et al., 2012a; Ma et al., 2012b; Hung et al., 2015) employed physisorption analysis which measured change in water vapor pressure caused by adsorption onto mineral dust (Ma et al., 2010b). Thermogravimetric analysis, physisorption analysis and the VSA technique used in our work can be considered as absolutely quantitative, and as discussed in Sections 3.2.1-3.2.6, in general our work agreed well with these four previous studies (Gustafsson et al., 2005; Ma et al., 2012a; Ma et al., 2012b; Hung et al., 2015).

FTIR was widely employed in previous work (Goodman et al., 2001; Frinak et al., 2005; Ma et al., 2010a; Joshi et al., 2017; Ibrahim et al., 2018) to study water uptake onto mineral dust, although it is not straightforward to convert IR absorption intensities of adsorbed water to its absolute amounts (Schuttlefield et al., 2007a; Ma et al., 2010b; Tang et al., 2019a). The relative differences between these studies and our work were typically within a factor of 2-3; since even for dust samples with the same name, samples examined in different studies may actually differ substantially in composition and water uptake properties, the agreement between these studies and our work can be considered as fairly good.

QCM is another technique widely used to investigate water uptake onto mineral dust (Schuttlefield et al., 2007b; Hatch et al., 2008; Schuttlefield, 2008; Navea et al., 2010; Hatch et al., 2011; Yeşilbaş and Boily, 2016). As shown in Section 3.2.1-3.2.6, though good agreement was found for some mineral dust between our work and these QCM studies, large discrepancies (up to 2-3 orders of magnitude) were frequently observed. This implies that the underlying assumptions required to convert the change in resonance frequency of the quartz crystal to the change in sample mass may not be fulfilled, and as a result the QCM results should be used with cautions.

For the same dust (at least with the same name), different samples with distinctive hygroscopicity may have been used in our work and previous studies, contributing to the observed discrepancies; in addition, previous work may adopt various pretreatment procedures, and it is difficult to assess the effects of these pretreatment on dust hygroscopicity reported in different studies. To further understand and resolve the discrepancies identified, it will be very useful to distribute the same samples to different groups (in which different techniques would be applied to study their hygroscopic properties) and compare the results obtained; furthermore, these samples should be pretreated with same or very similar protocols after received by different groups. Similar strategies have already been adopted before to compare different instruments used for ice nucleation research and shown to be valuable (Hiranuma et al., 2015; DeMott et al., 2018).

3.3 Hygroscopicity parameterizations

It has been suggested that water adsorption and hygroscopicity of insoluble particles can be parameterized as a function of RH by several theoretical models, including 1) the Brunauer-Emmet-Teller (BET) adsorption isotherm (Goodman et al., 2001; Ma et al., 2010a; Joshi et al., 2017; Ibrahim et al., 2018), 2) the Freundlich adsorption isotherm (Hatch et al., 2011), 3) Frenkel-Halsey-Hill (FHH) adsorption isotherm (Kumar et al., 2011b; Hatch et al., 2014; Hung et al., 2015; Hatch et al., 2019) and 4) the κ-Köhler equation (Chen et al., 2019; Tang et al., 2019b). In this work we attempted to use the aforementioned four models to fit our experimental data. As shown in Figure 10 (where SiO_2, albite, kaolinite and TLF dust are used as examples), our work suggested that the FHH adsorption isotherm could well describe the measured hygroscopicity of mineral dust samples as a function of RH. In addition, we found that other three parameterization methods could not fit our experimental data.

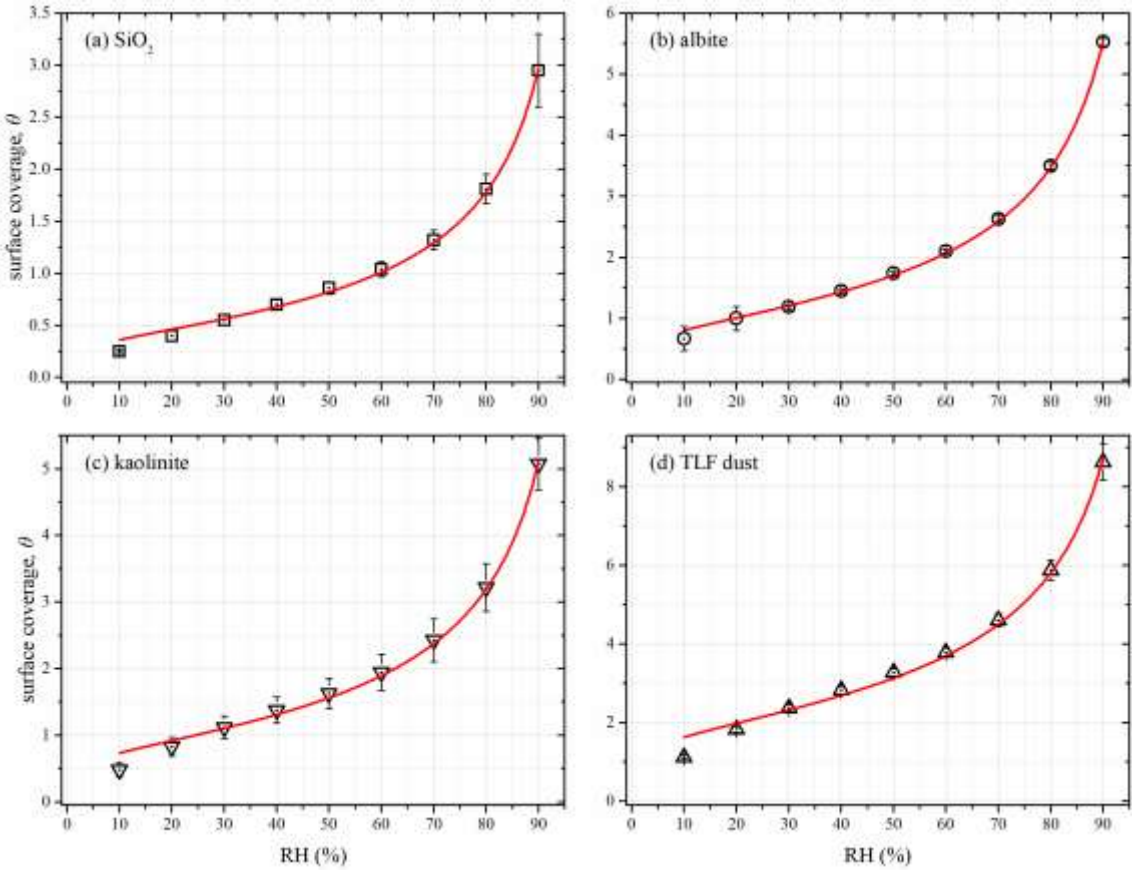

Figure 10. Surface coverages (θ) of adsorbed water on (a) SiO_2, (b) albite, (c) kaolinite and (d) TLF dust as a function of RH (0%-90%) at 25 °C. The experimental data were fitted with Frenkel-Halsey-Hill adsorption isotherm model (solid curves).

The FHH adsorption isotherm, which describes surface coverages of adsorbed water (θ) as a function of RH, is given by Eq. (2) (Sorjamaa and Laaksonen, 2007; Tang et al., 2016):

$$\theta = \sqrt[B_{FHH}]{\frac{A_{FHH}}{-\ln(RH)}} \qquad (2),$$

where A_{FHH} and B_{FHH} are empirical parameters. We found that Eq. (2) can well fit θ versus RH for all the 21 mineral dust samples examined (R^2 were found to be in the range of 0.94-0.99), and the generated A_{FHH} and B_{FHH} values are summarized in Table 6. As shown in Table 6, A_{FHH} values spanned from 0.15±0.01 (dolomite) to 4.39±0.81 (ATD), while the variation of B_{FHH} was much

smaller, ranging from 1.10 ±0.04 (for Bordj dust) to 1.91 ±0.18 (for ATD). Our results were largely consistent with the theoretical work by Sorjamaa and Laaksonen (2007), who suggested from a theoretical view that typical A_{FHH} and B_{FHH} values should be in the range of 0.1-3.0 and 0.5-3.0.

Table 6. Comparison A_{FHH} and B_{FHH} values determined in our work for mineral dust with those reported in previous studies ([a]: Kumar et al., 2011a; [b]: Hung et al., 2015; [c]: Hatch et al., 2019).

sample	A_{FHH}	B_{FHH}	sample	A_{FHH}	B_{FHH}
TiO_2	0.35 ±0.01	1.52 ±0.05	SiO_2	0.50 ±0.03	1.23 ±0.07
hematite	1.03 ±0.09	1.67 ±0.09		2.95 ±0.05 [a]	1.36 ±0.03 [a]
magnetite	0.41 ±0.01	1.33 ±0.03	$CaCO_3$	0.23 ±0.02	1.18 ±0.09
goethite	0.59 ±0.04	1.49 ±0.07		3.00 ±0.04 [a]	1.30 ±0.03 [a]
dolomite	0.15 ±0.01	1.43 ±0.07	illite	1.96 ±0.23	1.56 ±0.21
albite	1.68 ±0.02	1.61 ±0.01		1.02 ±0.38 [a]	1.12 ±0.04 [a]
potassium feldspar	1.10 ±0.06	1.42 ±0.09		2.06 [c]	2.19 [c]
microcline	1.22 ±0.05	1.17 ±0.03	kaolinite	1.24 ±0.10	1.48 ±0.08
chlorite	0.96 ±0.06	1.55 ±0.07		1.70 [b]	2.25 [b]
China loess	3.19 ±0.47	1.84 ±0.12	montmorillonite	0.65 ±0.05	1.13 ±0.07
QH dust	2.53 ±0.32	1.49 ±0.08		2.06 ±0.72 [a]	1.23 ±0.04 [a]
TLF dust	4.08 ±0.60	1.59 ±0.12		1.23 ±0.31 [a]	1.08 ±0.03 [a]
Bordj dust	0.49 ±0.03	1.10 ±0.04		1.25 [b]	1.33 [b]
M'Bour dust	0.59 ±0.05	1.27 ±0.09		2.28 [c]	1.45 [c]
Saharan dust	2.03 ±0.18	1.67 ±0.11	ATD	4.39 ±0.81	1.91 ±0.18
				2.96 ±0.03 [a]	1.28 ±0.03 [a]

A few previous studies investigated hygroscopic properties (Hung et al., 2015; Hatch et al., 2019) and CCN activities (Kumar et al., 2011b) of mineral dust, and reported A_{FHH} and B_{FHH} values for samples they examined. Their results are also compiled in Table 6. As revealed by Table 6, B_{FHH} values reported in our work were reasonably consistent with previous studies, while larger differences were observed for A_{FHH} values, especially between our study and the work by Kumar

et al. (2011a) for SiO_2 and $CaCO_3$. One reason for such large difference is that Kumar et al. (2011a) carried out their CCN activity measurements at >100% RH whereas our work on hygroscopic growth was conducted at <100% RH. Another study (Kumar et al., 2011a) reported A_{FHH} and B_{FHH} values for wet-generated mineral dust aerosols. Since the hygroscopicity of wet-generated mineral dust aerosols could be very different from dry-generated aerosols (Sullivan et al., 2010b; Kumar et al., 2011a), the results reported by Kumar et al. (2011b) for wet-generated aerosols are not further discussed.

4 Discussions

As shown in Tables 2-5, among the 21 mineral dust samples examined, $m_w(90\%)/m_0$ (mass ratios of adsorbed water at 90% RH to the dry sample) was found to range from 0.0011 for $CaCO_3$ to 0.0380 for montmorillonite, and $\theta(90\%)$ (surface coverages of adsorbed water at 90% RH) varied between 1.26 for dolomite and 8.63 for TLF dust. It appears that clay minerals and authentic mineral dust samples usually exhibited larger hygroscopicity on a per mass basis, when compared to other types of mineral dust. TiO_2, for which $m_w(90\%)/m_0$ was only lower than ATD, Saharan dust and montmorillonite, was an outstanding exception, probably because of its very large BET surface area (54.6 m^2 g^{-1}).

One may expect that on a per mass basis, mineral dust samples with larger surface area would have larger capacities to adsorb water. This was supported by our results shown in Figure 4a, which suggests that for mineral dust samples considered in our study, overall $m_w(90\%)/m_0$ increased with the BET surface area. Nevertheless, not all the samples obeyed this overall trend, as evident from Figure 4a, indicating that other factors would also play some roles in determining the ability of mineral dust to adsorb water on a per mass basis. We also explored if there was any relationship between hygroscopicity of mineral dust samples and soluble materials they contained. It was found

499 that for the 21 mineral dust samples considered in our work, $m_w(90\%)/m_0$ did not show any general
500 dependence on the amounts of soluble inorganic ions.

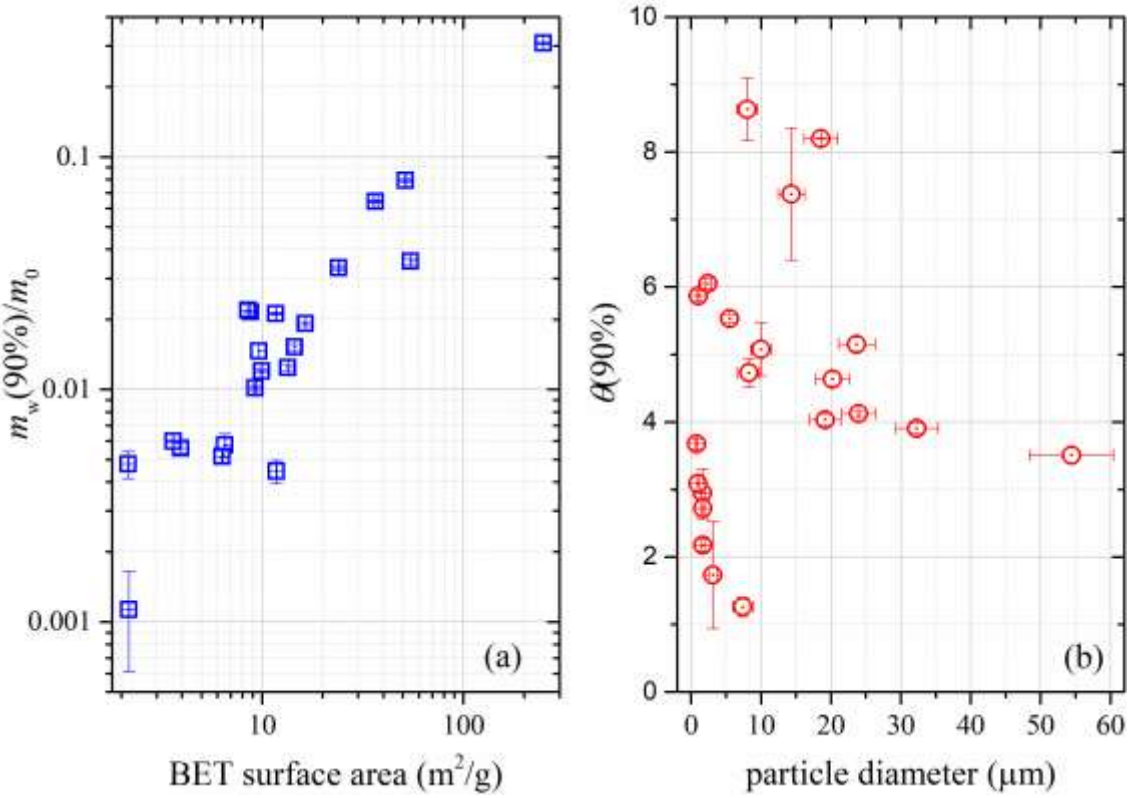

501

502 **Figure 11.** (a) The dependence of $m_w(90\%)/m_0$ (mass ratios of adsorbed water to the dry mineral
503 at 90% RH) on BET surface areas; (b) the dependence of $\theta(90\%)$ (surface coverages of adsorbed
504 water at 90% RH) on average particle diameters.

505

506 Ibrahim et al. (2018) studied water adsorption on ATD particles with different particle sizes,
507 and found that the RH at which one monolayer of adsorbed water was formed increased with
508 particle size; in other words, at the same RH the surface coverages of adsorbed water would be
509 higher for smaller particles (Ibrahim et al., 2018). In contrast, Yeşilbaş and Boily (2016)
510 investigated water adsorption on different mineral samples (21 in total), and suggested that at the
511 same RH more monolayers of adsorbed water would be formed on larger particles. However, as

shown in Figure 11b in which our measured θ at 90% RH are plotted versus particles size, our work revealed that surface coverages of adsorbed water at 90% RH showed no dependence on particle size for the 21 mineral dust samples examined in our work. This conclusion should be used with caution as dust samples used in our work were far from being monodisperse (see Figures S1-S7).

5 Conclusions

Hygroscopicity largely determines environmental and climatic effects of mineral dust aerosol, one of the most abundant tropospheric aerosols. However, hygroscopic properties of mineral dust remain highly uncertain, due to relatively low hygroscopicity of mineral dust and its non-sphericity. In our work, a vapor sorption analyzer, which measured sample mass as a function of RH (<1 to 90%), was employed to investigate water adsorption and hygroscopic properties of 21 different mineral dust samples, including seven authentic mineral dust samples (from Africa, China and America) and fourteen major minerals found in tropospheric mineral dust aerosol.

For all the mineral dust samples (21 in total) examined, $m_w(90\%)/m_0$ was found to range from 0.0011 ($CaCO_3$) to 0.3080 (montmorillonite), and $\theta(90\%)$ varied between 1.26 (dolomite) and 8.63 (TLF dust). When compared to other types of mineral dust, clay minerals and authentic mineral dust samples usually exhibited larger hygroscopicity on a per mass basis. Our work suggested that overall $m_w(90\%)/m_0$ increased with the BET surface area, indicating that on a per mass basis, mineral dust samples with larger surface area would have larger capacities to adsorb water in general. Our results revealed no dependence of $m_w(90\%)/m_0$ on the amount of soluble materials contained, or no dependence of $\theta(90\%)$ on particle size. In addition, it was found in our work that the Frenkel-Halsey-Hill (FHH) adsorption isotherm could well describe surface

coverages of adsorbed water as a function of RH for all the mineral dust investigated, and A_{FHH} and B_{FHH} parameters were determined to be in the range of 0.15-4.39 and 1.10-1.91, respectively.

Data availability. Data used in this paper can be found in the main text or supplement of this manuscript.

Competing interests. The authors declare that they have no conflict of interest.

Author contribution. Mingjin Tang conceived this work; Lanxiadi Chen, Chao Peng, Wenjun Gu, Hanjing Fu and Huanhuan Zhang carried out experiments under the advice of Xing Jian and Mingjin Tang; Lanxiadi Chen, Chao Peng, Athanasios Nenes and Mingjin Tang analyzed the data; Lanxiadi Chen, Chao Peng, Athanasios Nenes and Mingjin Tang wrote the manuscript with input from all the coauthors.

Financial support. This work was sponsored by National Natural Science Foundation of China (42022050 and 91744204), Ministry of Science and Technology of China (2018YFC0213901), Guangdong Foundation for Program of Science and Technology Research (2017B030314057 and 2019B121205006), Guangdong Province (2017GC010501) and the CAS Pioneer Hundred Talents program.

Acknowledgement. We would like to thank John Crowley (Max Planck Institute for Chemistry, Germany) for providing Saharan dust, Pingqing Fu (Tianjin University, China) for providing TLF dust, and Manolis Romanias (Université Lille, France) for providing M'Bour dust and Bordj dust.

Reference:

Attwood, A. R., and Greenslade, M. E.: Optical Properties and Associated Hygroscopicity of Clay Aerosols, Aerosol Sci. Technol., 45, 1350-1359, 2011.

Balkanski, Y., Schulz, M., Claquin, T., and Guibert, S.: Reevaluation of Mineral Aerosol Radiative Forcings Suggests a Better Agreement with Satellite and AERONET Data, Atmos. Chem. Phys., 7, 81-95, 2007.

559 Cases, J. M., Berend, I., Besson, G., Francois, M., Uriot, J. P., Thomas, F., and Poirier, J. E.: Mechanism of
560 adsorption and desorption of water vapor by homoionic montmorillonite. 1. The sodium-exchanged form, Langmuir,
561 8, 2730-2739, 1992.
562 Chen, L. X. D., Chen, Y. Z., Chen, L. L., Gu, W. J., Peng, C., Luo, S. X., Song, W., Wang, Z., and Tang, M. J.:
563 Hygroscopic properties of eleven pollen species in China, ACS Earth Space Chem., 3, 2678-2683, 2019.
564 Cziczo, D. J., Froyd, K. D., Hoose, C., Jensen, E. J., Diao, M., Zondlo, M. A., Smith, J. B., Twohy, C. H., and
565 Murphy, D. M.: Clarifying the Dominant Sources and Mechanisms of Cirrus Cloud Formation, Science, 340, 1320-
566 1324, 2013.
567 DeMott, P. J., Möhler, O., Cziczo, D. J., Hiranuma, N., Petters, M. D., Petters, S. S., Belosi, F., Bingemer, H. G.,
568 Brooks, S. D., Budke, C., Burkert-Kohn, M., Collier, K. N., Danielczok, A., Eppers, O., Felgitsch, L., Garimella, S.,
569 Grothe, H., Herenz, P., Hill, T. C. J., Höhler, K., Kanji, Z. A., Kiselev, A., Koop, T., Kristensen, T. B., Krüger, K.,
570 Kulkarni, G., Levin, E. J. T., Murray, B. J., Nicosia, A., O'Sullivan, D., Peckhaus, A., Polen, M. J., Price, H. C.,
571 Reicher, N., Rothenberg, D. A., Rudich, Y., Santachiara, G., Schiebel, T., Schrod, J., Seifried, T. M., Stratmann, F.,
572 Sullivan, R. C., Suski, K. J., Szakáll, M., Taylor, H. P., Ullrich, R., Vergara-Temprado, J., Wagner, R., Whale, T. F.,
573 Weber, D., Welti, A., Wilson, T. W., Wolf, M. J., and Zenker, J.: The Fifth International Workshop on Ice
574 Nucleation phase 2 (FIN-02): laboratory intercomparison of ice nucleation measurements, Atmos. Meas. Tech., 11,
575 6231-6257, 2018.
576 Di Biagio, C., Formenti, P., Balkanski, Y., Caponi, L., Cazaunau, M., Pangui, E., Journet, E., Nowak, S., Caquineau,
577 S., Andreae, M. O., Kandler, K., Saeed, T., Piketh, S., Seibert, D., Williams, E., and Doussin, J. F.: Global scale
578 variability of the mineral dust long-wave refractive index: a new dataset of in situ measurements for climate
579 modeling and remote sensing, Atmos. Chem. Phys., 17, 1901-1929, 2017.
580 Dupart, Y., King, S. M., Nekat, B., Nowak, A., Wiedensohler, A., Herrmann, H., David, G., Thomas, B., Miffre, A.,
581 Rairoux, P., D'Anna, B., and George, C.: Mineral dust photochemistry induces nucleation events in the presence of
582 SO2, Proc. Natl. Acad. Sci. U.S.A., 409, 20842-20847, 2012.
583 Engelbrecht, J. P., Moosmüller, H., Pincock, S., Jayanty, R. K. M., Lersch, T., and Casuccio, G.: Technical note:
584 Mineralogical, chemical, morphological, and optical interrelationships of mineral dust re-suspensions, Atmos.
585 Chem. Phys., 16, 10809-10830, 2016.
586 Formenti, P., Schutz, L., Balkanski, Y., Desboeufs, K., Ebert, M., Kandler, K., Petzold, A., Scheuvens, D.,
587 Weinbruch, S., and Zhang, D.: Recent progress in understanding physical and chemical properties of African and
588 Asian mineral dust, Atmos. Chem. Phys., 11, 8231-8256, 2011.
589 Frinak, E. K., Mashburn, C. D., Tolbert, M. A., and Toon, O. B.: Infrared characterization of water uptake by low-
590 temperature Na-montmorillonite: Implications for Earth and Mars, J. Geophys. Res.-Atmos., 110, D09308, doi:
591 09310.01029/02004JD005647, 2005.
592 Garimella, S., Huang, Y. W., Seewald, J. S., and Cziczo, D. J.: Cloud condensation nucleus activity comparison of
593 dry- and wet-generated mineral dust aerosol: the significance of soluble material, Atmos. Chem. Phys., 14, 6003-
594 6019, 2014.
595 Ginoux, P., Prospero, J. M., Gill, T. E., Hsu, N. C., and Zhao, M.: Global-scale Attribution of Anthropogenic and
596 Natural Dust Sources and Their Emission Rates Based on MODIS Deep Blue Aerosol Products, Rev. Geophys., 50,
597 RG3005, doi: 3010.1029/2012RG000388, 2012.
598 Goodman, A. L., Bernard, E. T., and Grassian, V. H.: Spectroscopic Study of Nitric Acid and Water Adsorption on
599 Oxide Particles: Enhanced Nitric Acid Uptake Kinetics in the Presence of Adsorbed Water, J. Phys. Chem. A, 105,
600 6443-6457, 2001.
601 Gu, W. J., Li, Y. J., Zhu, J. X., Jia, X. H., Lin, Q. H., Zhang, G. H., Ding, X., Song, W., Bi, X. H., Wang, X. M., and
602 Tang, M. J.: Investigation of water adsorption and hygroscopicity of atmospherically relevant particles using
603 a commercial vapor sorption analyzer, Atmos. Meas. Tech., 10, 3821-3832, 2017.
604 Gustafsson, R. J., Orlov, A., Badger, C. L., Griffiths, P. T., Cox, R. A., and Lambert, R. M.: A comprehensive
605 evaluation of water uptake on atmospherically relevant mineral surfaces: DRIFT spectroscopy, thermogravimetric
606 analysis and aerosol growth measurements, Atmos. Chem. Phys., 5, 3415-3421, 2005.
607 Hall, P. L., and Astill, D. M.: Adsorption of water by homoionic exchange forms of Wyoming Montmorillonite
608 (SWy-1), Clays and Clay Minerals, 37, 355-363, 1989.
609 Hatch, C. D., Gierlus, K. M., Schuttlefield, J. D., and Grassian, V. H.: Water adsorption and cloud condensation
610 nuclei activity of calcite and calcite coated with model humic and fulvic acids, Atmos. Environ., 42, 5672-5684,
611 2008.
612 Hatch, C. D., Wiese, J. S., Crane, C. C., Harris, K. J., Kloss, H. G., and Baltrusaitis, J.: Water Adsorption on Clay
613 Minerals As a Function of Relative Humidity: Application of BET and Freundlich Adsorption Models, Langmuir,
614 28, 1790-1803, 2011.

Hatch, C. D., Greenaway, A. L., Christie, M. J., and Baltrusaitis, J.: Water adsorption constrained Frenkel–Halsey–Hill adsorption activation theory: Montmorillonite and illite, Atmos. Environ., 87, 26-33, 2014.
Hatch, C. D., Tumminello, P. R., Cassingham, M. A., Greenaway, A. L., Meredith, R., and Christie, M. J.: Technical note: Frenkel, Halsey and Hill analysis of water on clay minerals: toward closure between cloud condensation nuclei activity and water adsorption, Atmos. Chem. Phys., 19, 13581-13589, 2019.
He, H., Wang, Y., Ma, Q., Ma, J., Chu, B., Ji, D., Tang, G., Liu, C., Zhang, H., and Hao, J.: Mineral Dust and NOx Promote the Conversion of SO_2 to Sulfate in Heavy Pollution Days, Sci. Rep., 4, 4172, 2014.
Herich, H., Tritscher, T., Wiacek, A., Gysel, M., Weingartner, E., Lohmann, U., Baltensperger, U., and Cziczo, D. J.: Water uptake of clay and desert dust aerosol particles at sub- and supersaturated water vapor conditions, Phys. Chem. Chem. Phys., 11, 7804-7809, 2009.
Hiranuma, N., Augustin-Bauditz, S., Bingemer, H., Budke, C., Curtius, J., Danielczok, A., Diehl, K., Dreischmeier, K., Ebert, M., Frank, F., Hoffmann, N., Kandler, K., Kiselev, A., Koop, T., Leisner, T., Möhler, O., Nillius, B., Peckhaus, A., Rose, D., Weinbruch, S., Wex, H., Boose, Y., DeMott, P. J., Hader, J. D., Hill, T. C. J., Kanji, Z. A., Kulkarni, G., Levin, E. J. T., McCluskey, C. S., Murakami, M., Murray, B. J., Niedermeier, D., Petters, M. D., O'Sullivan, D., Saito, A., Schill, G. P., Tajiri, T., Tolbert, M. A., Welti, A., Whale, T. F., Wright, T. P., and Yamashita, K.: A comprehensive laboratory study on the immersion freezing behavior of illite NX particles: a comparison of 17 ice nucleation measurement techniques, Atmos. Chem. Phys., 15, 2489-2518, 2015.
Huang, J. P., Wang, T. H., Wang, W. C., Li, Z. Q., and Yan, H. R.: Climate effects of dust aerosols over East Asian arid and semiarid regions, J. Geophys. Res.-Atmos., 119, 11398-11416, 2014.
Huneeus, N., Schulz, M., Balkanski, Y., Griesfeller, J., Prospero, J., Kinne, S., Bauer, S., Boucher, O., Chin, M., Dentener, F., Diehl, T., Easter, R., Fillmore, D., Ghan, S., Ginoux, P., Grini, A., Horowitz, L., Koch, D., Krol, M. C., Landing, W., Liu, X., Mahowald, N., Miller, R., Morcrette, J. J., Myhre, G., Penner, J., Perlwitz, J., Stier, P., Takemura, T., and Zender, C. S.: Global dust model intercomparison in AeroCom phase I, Atmos. Chem. Phys., 11, 7781-7816, 2011.
Hung, H. M., Wang, K. C., and Chen, J. P.: Adsorption of nitrogen and water vapor by insoluble particles and the implication on cloud condensation nuclei activity, J. Aerosol. Sci., 86, 24-31, 2015.
Ibrahim, S., Romanias, M. N., Alleman, L. Y., Zeineddine, M. N., Angeli, G. K., Trikalitis, P. N., and Thevenet, F.: Water Interaction with Mineral Dust Aerosol: Particle Size and Hygroscopic Properties of Dust, ACS Earth and Space Chem., 2, 376-386, 2018.
Jickells, T. D., An, Z. S., Andersen, K. K., Baker, A. R., Bergametti, G., Brooks, N., Cao, J. J., Boyd, P. W., Duce, R. A., Hunter, K. A., Kawahata, H., Kubilay, N., laRoche, J., Liss, P. S., Mahowald, N., Prospero, J. M., Ridgwell, A. J., Tegen, I., and Torres, R.: Global Iron Connections between Desert Dust, Ocean Biogeochemistry, and Climate, Science, 308, 67-71, 2005.
Joshi, N., Romanias, M. N., Riffault, V., and Thevenet, F.: Investigating water adsorption onto natural mineral dust particles: Linking DRIFTS experiments and BET theory, Aeolian Res., 27, 35-45, 2017.
Journet, E., Balkanski, Y., and Harrison, S. P.: A New Data Set of Soil Mineralogy for Dust-cycle Modeling, Atmos. Chem. Phys., 14, 3801-3816, 2014.
Karydis, V. A., Tsimpidi, A. P., Bacer, S., Pozzer, A., Nenes, A., and Lelieveld, J.: Global impact of mineral dust on cloud droplet number concentration, Atmos. Chem. Phys., 17, 5601-5621, 2017.
Ketteler, G., Yamamoto, S., Bluhm, H., Andersson, K., Starr, D. E., Ogletree, D. F., Ogasawara, H., Nilsson, A., and Salmeron, M.: The Nature of Water Nucleation Sites on TiO2(110) Surfaces Revealed by Ambient Pressure X-ray Photoelectron Spectroscopy, J. Phys. Chem. C, 111, 8278-8282, 2007.
Knippertz, P., and Stuut, J. B. W.: Mineral Dust: A Key Player in the Earth System, Springer, Dordrecht, 2014.
Koehler, K. A., Kreidenweis, S. M., DeMott, P. J., Petters, M. D., Prenni, A. J., and Carrico, C. M.: Hygroscopicity and cloud droplet activation of mineral dust aerosol, Geophys. Res. Lett., 36, L08805, doi: 08810.01029/02009gl037348, 2009.
Kreidenweis, S. M., and Asa-Awuku, A.: 5.13 - Aerosol Hygroscopicity: Particle Water Content and Its Role in Atmospheric Processes, in: Treatise on Geochemistry (Second Edition), edited by: Turekian, K. K., Elsevier, Oxford, 331-361, 2014.
Kumar, P., Sokolik, I. N., and Nenes, A.: Parameterization of cloud droplet formation for global and regional models: including adsorption activation from insoluble CCN, Atmos. Chem. Phys., 9, 2517-2532, 2009.
Kumar, P., Sokolik, I. N., and Nenes, A.: Cloud condensation nuclei activity and droplet activation kinetics of wet processed regional dust samples and minerals, Atmos. Chem. Phys., 11, 8661-8676, 2011a.
Kumar, P., Sokolik, I. N., and Nenes, A.: Measurements of cloud condensation nuclei activity and droplet activation kinetics of fresh unprocessed regional dust samples and minerals, Atmos. Chem. Phys., 11, 3527-3541, 2011b.

Laaksonen, A., Malila, J., Nenes, A., Hung, H. M., and Chen, J. P.: Surface fractal dimension, water adsorption efficiency, and cloud nucleation activity of insoluble aerosol, Sci. Rep., 6, 25504, doi: 25510.21038/srep25504, 2016.
Lasne, J., Romanias, M. N., and Thevenet, F.: Ozone Uptake by Clay Dusts under Environmental Conditions, Acs Earth and Space Chemistry, 2, 904-914, 2018.
Li, R., Jia, X. H., Wang, F., Ren, Y., Wang, X., Zhang, H. H., Li, G. H., Wang, X. M., and Tang, M. J.: Heterogeneous reaction of NO2 with hematite, goethite and magnetite: Implications for nitrate formation and iron solubility enhancement, Chemosphere, 242, 125273, 2020.
Li, W. J., Xu, L., Liu, X. H., Zhang, J. C., Lin, Y. T., Yao, X. H., Gao, H. W., Zhang, D. Z., Chen, J. M., Wang, W. X., Harrison, R. M., Zhang, X. Y., Shao, L. Y., Fu, P. Q., Nenes, A., and Shi, Z. B.: Air pollution–aerosol interactions produce more bioavailable iron for ocean ecosystems, Science Adv., 3, e1601749, 2017.
Ma, Q. X., He, H., and Liu, Y. C.: In Situ DRIFTS Study of Hygroscopic Behavior of Mineral Aerosol, J. Environ. Sci., 22, 555-560, 2010a.
Ma, Q. X., Liu, Y. C., and He, H.: The Utilization of Physisorption Analyzer for Studying the Hygroscopic Properties of Atmospheric Relevant Particles, J. Phys. Chem. A, 114, 4232-4237, 2010b.
Ma, Q. X., Liu, Y. C., Liu, C., and He, H.: Heterogeneous Reaction of Acetic Acid on MgO, α-Al_2O_3, and $CaCO_3$ and the Effect on the Hygroscopic Behavior of These Particles, Phys. Chem. Chem. Phys., 14, 8403-8409, 2012a.
Ma, Q. X., Liu, Y. C., Liu, C., Ma, J. Z., and He, H.: A case study of Asian dust storm particles: Chemical composition, reactivity to SO2 and hygroscopic properties, J. Environ. Sci., 24, 62-71, 2012b.
Meskhidze, N., Volker, C., Al-Abadleh, H. A., Barbeau, K., Bressac, M., Buck, C., Bundy, R. M., Croot, P., Feng, Y., Ito, A., Johansen, A. M., Landing, W. M., Mao, J. Q., Myriokefalitakis, S., Ohnemus, D., Pasquier, B., and Ye, Y.: Perspective on identifying and characterizing the processes controlling iron speciation and residence time at the atmosphere-ocean interface, Mar. Chem., 217, 103704, doi: 103710.101016/j.marchem.102019.103704, 2019.
Mitroo, D., Gill, T. E., Haas, S., Pratt, K. A., and Gaston, C. J.: ClNO2 production from N2O5 uptake on saline playa dusts: New insights into potential inland sources of ClNO2, Environ. Sci. Technol., 13, 7442-7452, 2019.
Navea, J. G., Chen, H. H., Huang, M., Carmichael, G. R., and Grassian, V. H.: A comparative evaluation of water uptake on several mineral dust sources, Environ. Chem., 7, 162-170, 2010.
Nickovic, S., Vukovic, A., Vujadinovic, M., Djurdjevic, V., and Pejanovic, G.: Technical Note: High-resolution mineralogical database of dust-productive soils for atmospheric dust modeling, Atmos. Chem. Phys., 12, 845-855, 2012.
Okin, G. S., Baker, A. R., Tegen, I., Mahowald, N. M., Dentener, F. J., Duce, R. A., Galloway, J. N., Hunter, K., Kanakidou, M., Kubilay, N., Prospero, J. M., Sarin, M., Surapipith, V., Uematsu, M., and Zhu, T.: Impacts of atmospheric nutrient deposition on marine productivity: Roles of nitrogen, phosphorus, and iron, Glob. Biogeochem. Cycle, 25, GB2022, doi: 2010.1029/2010GB003858, 2011.
Rubasinghege, G., and Grassian, V. H.: Role(s) of Adsorbed Water in the Surface Chemistry of Environmental Interfaces, Chem. Commun., 49, 3071-3094, 2013.
Scanza, R. A., Mahowald, N., Ghan, S., Zender, C. S., Kok, J. F., Liu, X., Zhang, Y., and Albani, S.: Modeling Dust as Component Minerals in the Community Atmosphere Model: Development of Framework and Impact on Radiative Forcing, Atmos. Chem. Phys., 15, 537-561, 2015.
Schulz, M., Prospero, J. M., Baker, A. R., Dentener, F., Ickes, L., Liss, P. S., Mahowald, N. M., Nickovic, S., Garc á-Pando, C. P., Rodr guez, S., Sarin, M., Tegen, I., and Duce, R. A.: Atmospheric Transport and Deposition of Mineral Dust to the Ocean: Implications for Research Needs, Environ. Sci. Technol., 46, 10390-10404, 2012.
Schuttlefield, J., Al-Hosney, H., Zachariah, A., and Grassian, V. H.: Attenuated Total Reflection Fourier Transform Infrared Spectroscopy to Investigate Water Uptake and Phase Transitions in Atmospherically Relevant Particles, Appl. Spectrosc., 61, 283-292, 2007a.
Schuttlefield, J. D., Cox, D., and Grassian, V. H.: An investigation of water uptake on clays minerals using ATR-FTIR spectroscopy coupled with quartz crystal microbalance measurements, J. Geophys. Res.-Atmos., 112, D21303, doi: 21310.21029/22007JD008973, 2007b.
Schuttlefield, J. D.: Laboratory Studies of Reactions of Atmospheric Gases with Components of Mineral Dust Aerosol and Research in Chemical Education, Ph. D., University of Iowa, 2008.
Sorjamaa, R., and Laaksonen, A.: The effect of H_2O adsorption on cloud drop activation of insoluble particles: a theoretical framework, Atmos. Chem. Phys., 7, 6175-6180, 2007.
Sullivan, R. C., Minambres, L., DeMott, P. J., Prenni, A. J., Carrico, C. M., Levin, E. J. T., and Kreidenweis, S. M.: Chemical processing does not always impair heterogeneous ice nucleation of mineral dust particles, Geophys. Res. Lett., 37, L24805, doi: 24810.21029/22010GL045540, 2010a.

Sullivan, R. C., Moore, M. J. K., Petters, M. D., Kreidenweis, S. M., Qafoku, O., Laskin, A., Roberts, G. C., and Prather, K. A.: Impact of Particle Generation Method on the Apparent Hygroscopicity of Insoluble Mineral Particles, Aerosol Sci. Technol., 44, 830-846, 2010b.
Tagliabue, A., Bowie, A. R., Boyd, P. W., Buck, K. N., Johnson, K. S., and Saito, M. A.: The integral role of iron in ocean biogeochemistry, Nature, 543, 51-59, 2017.
Tang, M. J., Thieser, J., Schuster, G., and Crowley, J. N.: Kinetics and Mechanism of the Heterogeneous Reaction of N_2O_5 with Mineral Dust Particles, Phys. Chem. Chem. Phys., 14, 8551-8561, 2012.
Tang, M. J., Schuster, G., and Crowley, J. N.: Heterogeneous Reaction of N_2O_5 with Illite and Arizona Test Dust Particles, Atmos. Chem. Phys., 14, 245-254, 2014.
Tang, M. J., Cziczo, D. J., and Grassian, V. H.: Interactions of Water with Mineral Dust Aerosol: Water Adsorption, Hygroscopicity, Cloud Condensation and Ice Nucleation, Chem. Rev., 116, 4205–4259, 2016.
Tang, M. J., Huang, X., Lu, K. D., Ge, M. F., Li, Y. J., Cheng, P., Zhu, T., Ding, A. J., Zhang, Y. H., Gligorovski, S., Song, W., Ding, X., Bi, X. H., and Wang, X. M.: Heterogeneous reactions of mineral dust aerosol: implications for tropospheric oxidation capacity, Atmos. Chem. Phys., 17, 11727-11777, 2017.
Tang, M. J., Chan, C. K., Li, Y. J., Su, H., Ma, Q. X., Wu, Z. J., Zhang, G. H., Wang, Z., Ge, M. F., Hu, M., He, H., and Wang, X. M.: A review of experimental techniques for aerosol hygroscopicity studies, Atmos. Chem. Phys., 19, 12631-12686, 2019a.
Tang, M. J., Gu, W. J., Ma, Q. X., Li, Y. J., Zhong, C., Li, S., Yin, X., Huang, R. J., He, H., and Wang, X. M.: Water adsorption and hygroscopic growth of six anemophilous pollen species: the effect of temperature, Atmos. Chem. Phys., 19, 2247-2258, 2019b.
Tang, M. J., Zhang, H. H., Gu, W. J., Gao, J., Jian, X., Shi, G. L., Zhu, B. Q., Xie, L. H., Guo, L. Y., Gao, X. Y., Wang, Z., Zhang, G. H., and Wang, X. M.: Hygroscopic Properties of Saline Mineral Dust From Different Regions in China: Geographical Variations, Compositional Dependence, and Atmospheric Implications, J. Geophys. Res.-Atmos, 124, 10844-10857, 2019c.
Textor, C., Schulz, M., Guibert, S., Kinne, S., Balkanski, Y., Bauer, S., Berntsen, T., Berglen, T., Boucher, O., Chin, M., Dentener, F., Diehl, T., Easter, R., Feichter, H., Fillmore, D., Ghan, S., Ginoux, P., Gong, S., Grini, A., Hendricks, J., Horowitz, L., Huang, P., Isaksen, I., Iversen, I., Kloster, S., Koch, D., Kirkevåg, A., Kristjansson, J. E., Krol, M., Lauer, A., Lamarque, J. F., Liu, X., Montanaro, V., Myhre, G., Penner, J., Pitari, G., Reddy, S., Seland, Ø., Stier, P., Takemura, T., and Tie, X.: Analysis and Quantification of the Diversities of Aerosol Life Cycles within AeroCom, Atmos. Chem. Phys., 6, 1777-1813, 2006.
Usher, C. R., Michel, A. E., and Grassian, V. H.: Reactions on Mineral Dust, Chem. Rev., 103, 4883-4939, 2003.
Vlasenko, A., Sjogren, S., Weingartner, E., Gaggeler, H. W., and Ammann, M.: Generation of submicron Arizona test dust aerosol: Chemical and hygroscopic properties, Aerosol Sci. Technol., 39, 452-460, 2005.
Vlasenko, A., Huthwelker, T., Gaggeler, H. W., and Ammann, M.: Kinetics of the heterogeneous reaction of nitric acid with mineral dust particles: an aerosol flow tube study, Phys. Chem. Chem. Phys., 11, 7921-7930, 2009.
Wang, T., Liu, Y., Deng, Y., Fu, H., Zhang, L., and Chen, J.: Adsorption of SO2 on mineral dust particles influenced by atmospheric moisture, Atmos. Environ., 191, 153-161, 2018.
Xu, W. Z., Johnston, C. T., Parker, P., and Agnew, S. F.: Infrared study of water sorption on Na-, Li-, Ca-, and Mg-exchanged (SWy-1 and SAz-1) montmorillonite, Clays Clay Miner., 48, 120-131, 2000.
Yeşilbaş, M., and Boily, J.-F.: Particle Size Controls on Water Adsorption and Condensation Regimes at Mineral Surfaces, Sci. Rep., 6, 32136, doi: 32110.31038/srep32136, 2016.
Yu, Z., and Jang, M.: Simulation of heterogeneous photooxidation of SO2 and NOx in the presence of Gobi Desert dust particles under ambient sunlight, Atmos. Chem. Phys., 18, 14609-14622, 2018.
Yu, Z., and Jang, M.: Atmospheric Processes of Aromatic Hydrocarbons in the Presence of Mineral Dust Particles in an Urban Environment, ACS Earth and Space Chemistry, 3, 2404-2414, 2019.
Zent, A. P., Howard, D. J., and Quinn, R. C.: H2O adsorption on smectites: Application to the diurnal variation of H2O in the Martian atmosphere, J. Geophys. Res.-Planets, 106, 14667-14674, 2001.